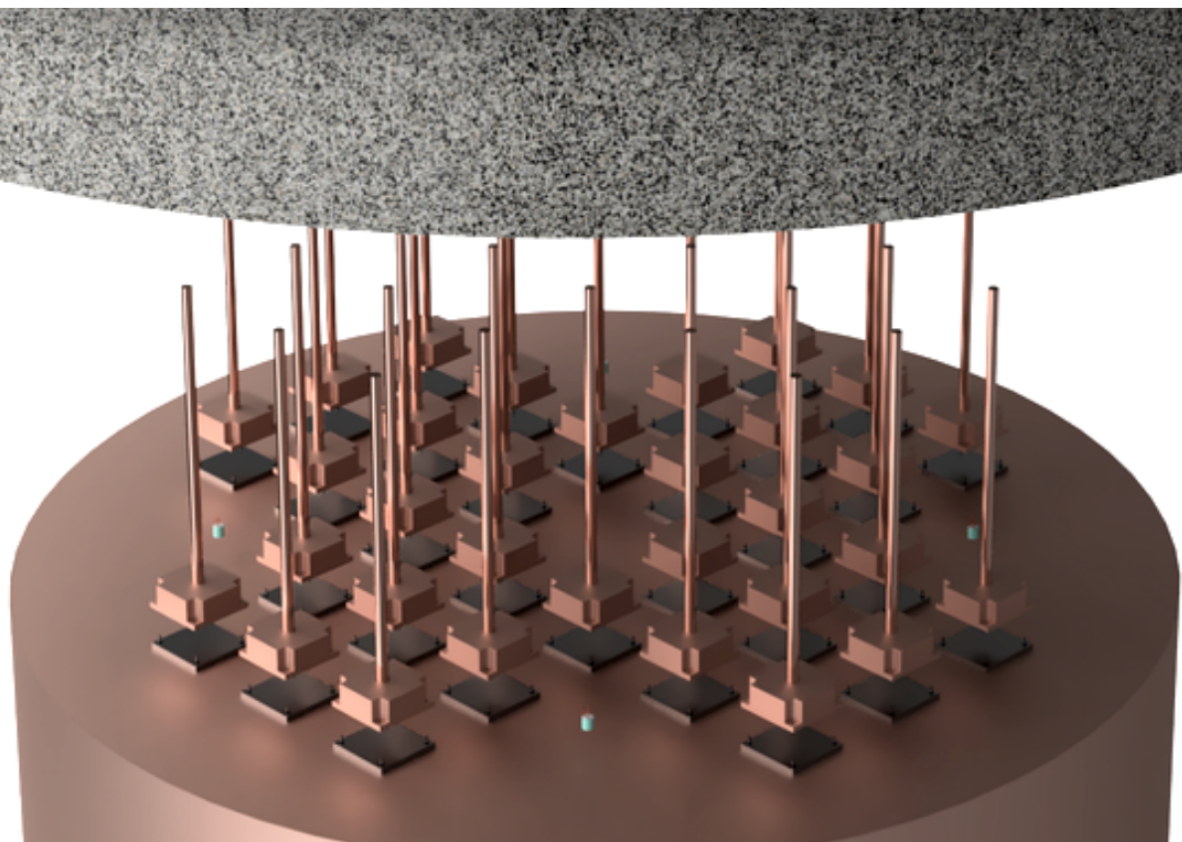


AUTOMATED LEAK DETECTION FOR NUCLEAR WASTE



Harry Rudd z5361096 -
h.rudd@student.unsw.edu.au

Peter Crosby z5363047 -
peter.crosby@student.unsw.edu.au

Kelly Huang z5361857 -
kelly.huang1@student.unsw.edu.au

Ben Kernohan z5359839 -
b.kernohan@student.unsw.edu.au

Daniel Arena z5361677 -
daniel.arena@student.unsw.edu.au

Marcus Borscz z5312512 -
m.borscz@student.unsw.edu.au

Jordan Whittaker z5363798 -
jordan.whittaker@student.unsw.edu.au

Executive Summary

The amount of high level nuclear waste is expected to increase by 75% by the year 2050, which will place a significant burden on current methods of reliably storing and monitoring spent fuel. High level nuclear waste will remain hazardous for thousands of years, posing harmful health and environmental risks if exposed to civilisation or natural ecosystems. Deep geological repositories will serve as a permanent burial ground for nuclear waste, and the most advanced facility ‘Onkalo’ in Finland is expected to be operational by 2023. However, public acceptance and concerns remain an issue, prohibiting the siting and operation of nuclear disposal facilities around the world. Increasing the community's confidence in nuclear waste disposal methods is therefore a priority for reducing our reliance on above-ground storage and improving the public image of the nuclear industry.

The solution is to design a self-sustained automated leak-detection system. Although there are many methods for nuclear waste radiation sensing, the system outlined in this report is unique to the extreme environment of deep geological repositories. It harvests the thermal energy from the decay heat to sufficiently power the radiation sensors and communication system into the service tunnels. The decision to harvest the nuclear thermal energy provides facility operators with the unprecedented capability of remotely monitoring the nuclear waste post-deposition. This allows them to identify whether a waste canister has been compromised and to provide evidence of safe and secure storage to the public and regulators.

This report will reflect on the design process and demonstrate the use of the Axiomatic Design Theory for concept generation and final design creation. It will also provide a technical analysis of the radiation sensor, which consists of a LYSO scintillator crystal and silicon photomultiplier. In principle, our sensor can identify radionuclide signatures, including those due to foreign material entering the waste package. The selection of materials for optimal thermal power generation is also analysed in this report. It found that a 34.51K temperature difference could be established across each thermoelectric generator, producing approximately 32W of power for the entire system.

CAD models and mechanical part drawings are also provided at the end of this report. A complete Bill of Materials shows that the cost per monitoring device is approximately \$2990.

Table of Contents

Executive Summary	2
Table of Contents	3
Team Statement	4
1. Introduction	5
1.1 Nuclear Background and Significance	5
1.2 Project Progress and Current Stage	6
1.3 Report Structure	7
2. Reflection on Conceptual Design	8
2.1 Initial Steps of the Design Process	8
2.2 Generation of Independence Matrix	9
2.3 Analysis of initial independence matrix	10
2.4 Proposed refactoring of design	11
2.5 Refactored design	11
2.7 Reflection on using the Independence Axiom	13
2.8 Impact of Independence Axiom on Design concepts	13
3. Technical Design and Analysis	14
3.1 Sensors	14
3.1.1 <i>The Radiation Sensor</i>	14
3.1.1.1 <i>Scintillation Detection</i>	14
3.1.1.2 <i>SiPM and Discriminator Biassing Circuit Design</i>	16
3.1.1.3 <i>Microcontroller</i>	17
3.1.2 <i>Scintillator Crystal Selection</i>	18
3.1.3 <i>Algorithm design for Scintillation System</i>	19
3.1.4 <i>Power Analysis for the Radiation Sensor</i>	20
3.2 Material Selection	22
3.2.1 <i>Thermal Requirements of Materials</i>	22
3.2.1.1 <i>Thermally Connecting Rock to TEGs</i>	23
3.2.1.2 <i>Thermal Isolation</i>	27
3.2.2 <i>Strength Requirements of Materials</i>	28
3.2.3 <i>Non-Epoxy Material for Circuitry</i>	29
4. CAD Model and Mechanical Part Drawing	31
5. Conclusion	37
References	38
Biography	39
Appendix	40
A1. Bill of Materials	40

Team Statement

All team members contributed consistent effort towards the project throughout the preliminary and final stages. Assigned responsibilities were completed in a timely manner by all members, and all team members maintained communication in regards to the final report through attendance in meetings and discussions. In respect to this report, sections were delegated with consideration of expertise and workload as follows:

- Kelly Huang: *Executive Summary/Title Page, Introduction, Technical Design and Analysis (Sensors), Conclusion*
- Ben Kernohan: *Conceptual Design*
- Daniel Arena: *Technical Design and Analysis (Sensors and Material Selection)*
- Harry Rudd: *Technical Design and Analysis (Material Selection)*
- Peter Crosby: *Technical Design and Analysis (Material Selection)*
- Jordan Whittaker: *Technical Design and Analysis (Thermal Material Selection), Computer Aided Mechanical Models*
- Marcus Borscz: *Computer Aided Mechanical Models and Mechanical Drawing*

1. Introduction

1.1 Nuclear Background and Significance

Nuclear energy is a low emission power source generated by the process of fission, whereby uranium atoms are split to produce energy. Currently, over 400 commercial nuclear power plants worldwide have the capacity to produce up to 400 GW of electricity, sufficient to power about 400 million households.[1] Globally, nuclear energy accounts for 9.9% of electricity generation[2], classifying it as the second largest source of low-carbon energy, behind hydropower. Figure 1. Exhibits the share of low-carbon sources and coal in world electricity generation, with nuclear energy taking the largest share at 2021.

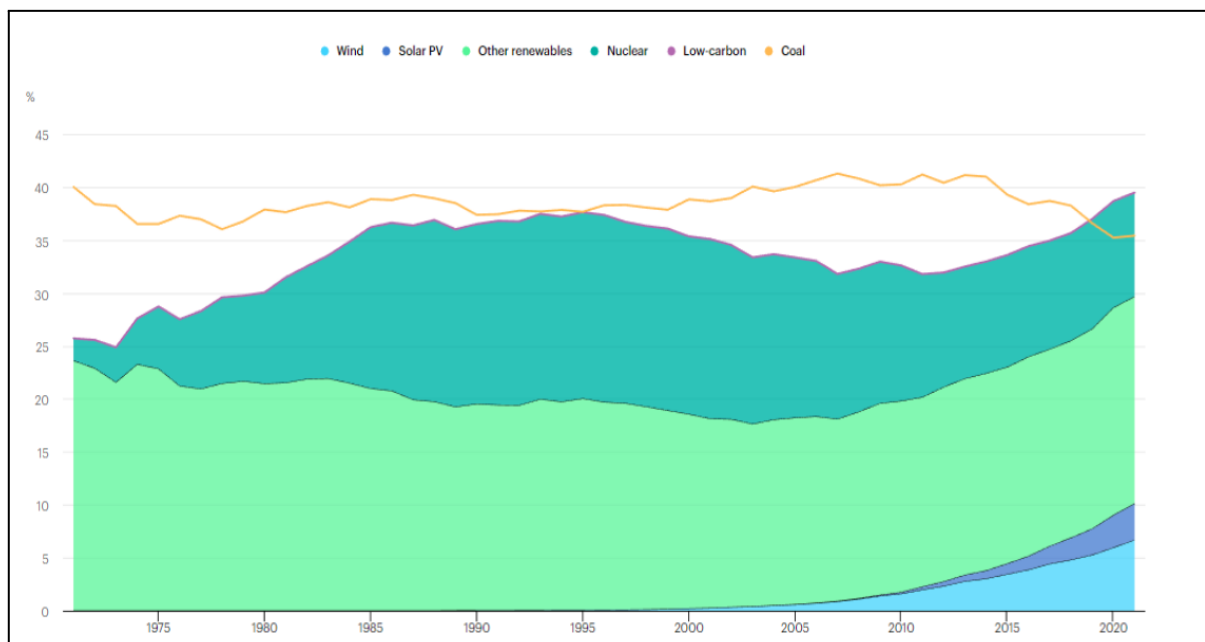


Figure 1. Share of low-carbon sources and coal in world electricity generation, 1971-2021 (IEA 2021)

The ambition to reach net-zero in carbon dioxide emissions by the year 2050 is currently in place, and to meet the International Energy Agency's *Net Zero Scenario*, nuclear power must double from 413 GW in 2022 to 812 GW in 2050[3]. Further, with commitments from 44 countries and the European Union to limit global warming by 1.5°C by 2050 in line with the Paris Agreement, the Intergovernmental Panel on Climate Change anticipates a 90% increase in nuclear power, with some models predicting a 305% increase.

However, with the increased use of nuclear energy the amount of high level nuclear waste (HLW) stored globally is expected to increase from 400 000 tonnes in 2022 to 700 000 tonnes in 2050[4]. HLW includes spent reactor fuel and waste materials from nuclear weapons manufacturing and is sufficiently radioactive, requiring both shielding and cooling. It contains a high level of alpha-emitting isotopes and due to

the long half-life of some radioisotopes, the waste must be managed for up to 100 000 years.

The current solution to manage the nuclear waste consists of deep geological repositories, with the most advanced plans implemented in countries including Finland, Sweden, France and the United States of America. Figure 2. Illustrates the repository 'Onkalo' in Finland, with expectations for the facility to be in operation by 2023. However, with the general perception of the dangers associated with radioactive waste, in conjunction with its negative portrayal in media and its false association with nuclear weapons, acceptance and confidence remains an issue. An example was evident in France, where street protests hindered plans for a disposal site to be implemented.[5]

Hence, the mission is to design a self-sustained automated leak detection system with the intention to increase confidence and reduce community concerns to encourage government investment in further permanent repositories.

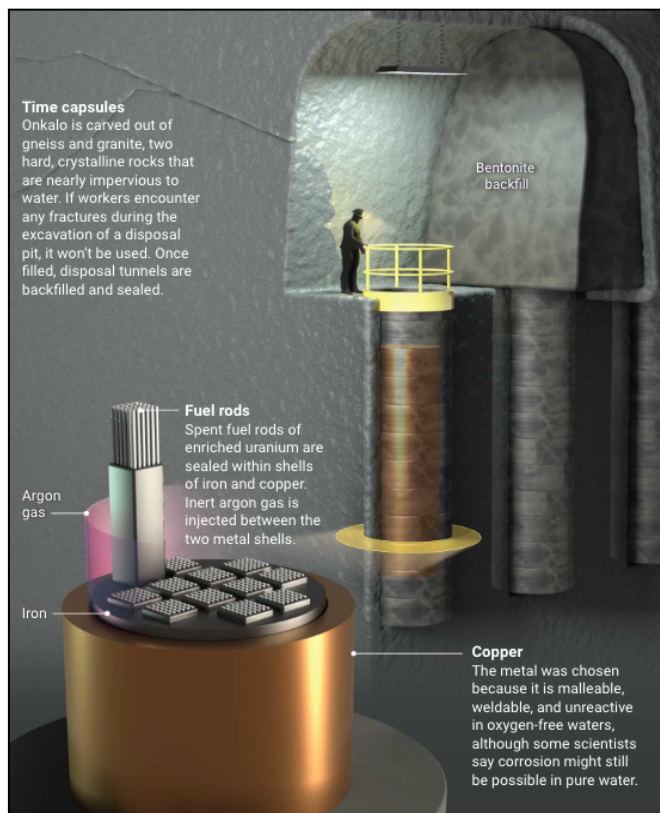


Figure 2. Finland's Deep Geological Repository, 'Onkalo'

1.2 Project Progress and Current Stage

The preliminary stages of the project involved research regarding the gap in the market, that is, the absence of monitoring systems in place for permanent nuclear waste storage. Establishing the aforementioned gap allowed the identification of multiple stakeholders which branched the project to consider the various customer

needs. These customer needs were then taken to develop functional requirements and design parameters and constraints. The project thus progressed into concept generation, with methods such as a morph evaluation matrix and the independence axiom theory applied to optimise the design. Computer aided design (CAD) models were altered and enhanced in the process for visualisation and performance purposes. The current stage consists of a finalised design solution that takes into consideration the functional requirements of utmost importance.

1.3 Report Structure

This report delves into the conceptual design phase, outlining the application of axiomatic design, in particular the Independence Axiom. The technical design and analysis focuses on sensors and material selection relevant to the design. Computer Aided Mechanical drawings and models are presented in Section 4 also, illustrating the final design solution.

2. Reflection on Conceptual Design

This section will discuss how the design process was followed and it will outline how Axiomatic Design Theory was applied to the design, specifically the use of the Independence Axiom.

2.1 Initial Steps of the Design Process

In the creation of the Unique Value Proposition (UVP), key customer needs (CN) and design constraints (DC) were found. In breaking these down, the functional requirements (FR) for a successful design were determined.

Customer Needs		Functional Requirements		
CN ₁	Information on capsule's storage condition	FR ₁	monitor condition of nuclear waste	FR ₁₁ Focus on a section of the capsule FR ₁₂ Measure condition of that section FR ₁₃ Compare with a previous measurement FR ₁₄ Determine if there is waste leakage FR ₂₁ Compute message to be transmitted FR ₂₂ Transmit message out of capsule borehole
			communicate information from capsule	FR ₂₃ Transmit message to surface FR ₂₄ Receive message at surface FR ₂₅ Interpret and read message
		FR ₃	Harvest Energy from capsule heat	FR ₃₁ Absorb decay heat FR ₃₂ Convert decay heat to electricity FR ₃₃ Dissipate heat into surroundings
				FR ₄₁ Protect energy harvesting device
				FR ₄₂ Protect sensors FR ₄₃ Protect communications FR ₄₄ Protect housing and fasteners
	CN ₂	FR ₄	Protect system from radiation	FR ₄₁ Protect energy harvesting device
				FR ₄₂ Protect sensors
				FR ₄₃ Protect communications
				FR ₄₄ Protect housing and fasteners
CN ₃	Logevity of operation			

Table 2.1.1 - Breakdown of functional requirements

Represented in Table 2.1.1 are the Functional Requirements, denoted FR_{xy}. These are a set of the lowest form of FRs in the design that must be satisfied for the design to be deemed successful. After generating these, initial design concepts were pieced together.

By the time of the Interim Presentation, the design had reached its first milestone - a full CAD model of the ideated system. From this model the initial Design Parameters (DP) were created based on the features that the design covered. This is shown in Figure 2.1.2.

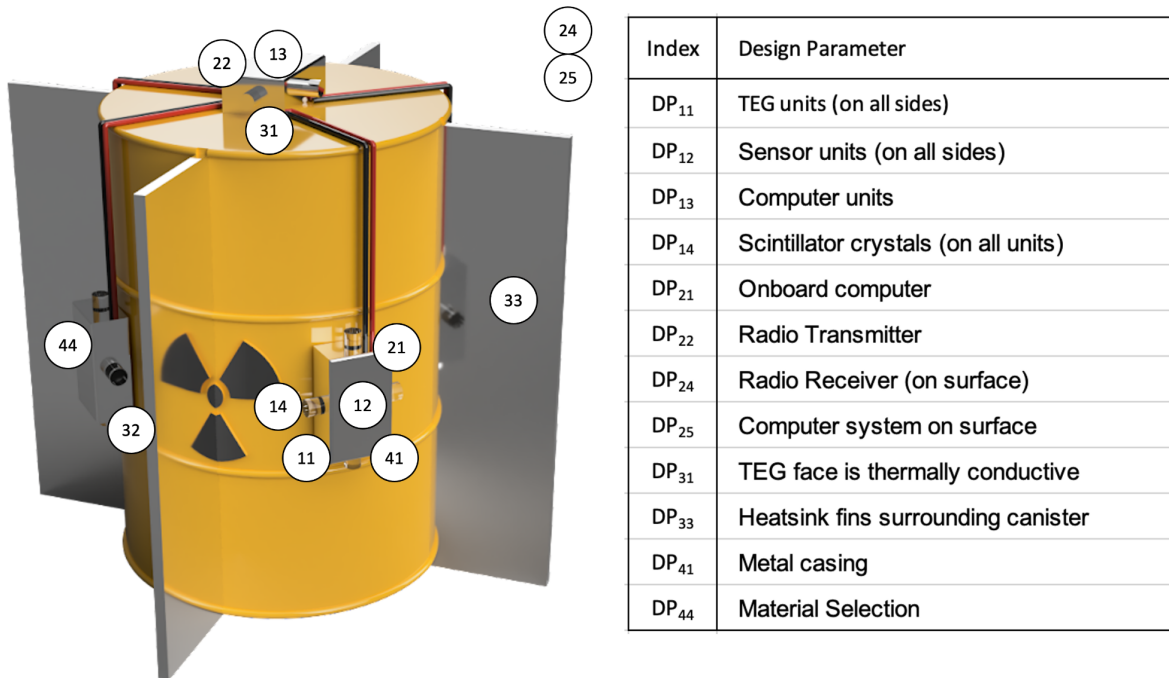


Figure 2.1.2 - Design Parameters (DP) of initial design

2.2 Generation of Independence Matrix

After determining the DPs of the system, a matrix was created to visually represent the Independence Axiom. This matrix was the initial step in determining the degree of coupling that existed in the design.

	DP ₁₁	DP ₁₂	DP ₁₃	DP ₁₄	DP ₂₁	DP ₂₂	DP ₂₄	DP ₂₅	DP ₃₁	DP ₃₃	DP ₄₁	DP ₄₄
FR ₁₁	X	X		X							X	
FR ₁₂		X				X						
FR ₁₃			X									
FR ₁₄				X								
FR ₂₁		X				X						
FR ₂₂							X					
FR ₂₃								X				
FR ₂₄								X				
FR ₂₅									X			
FR ₃₁										X		
FR ₃₂	X										X	
FR ₃₃											X	
FR ₄₁											X	
FR ₄₂											X	
FR ₄₃											X	
FR ₄₄												X

Table 2.2.1 - Matrix representation of the Independence Axiom applied on the Initial Design

2.3 Analysis of initial independence matrix

The number of DPs was less than the FRs. This was an indication that the design was coupled. In Table 2.2.1, coloured yellow are particular aspects that resulted in the design being decoupled. That is, when a given FR is satisfied by multiple DPs or where one DP satisfies multiple FRs. Further analysis of the subsystems in the design was necessary to determine where the design was coupled.

Isolating particular FR - DR relationships, it became evident which subsystems and areas of the design were coupled.

	DP ₁₁ TEG units on all sides	DP ₁₂ sensor units on all sides	DP ₁₄ Scintillator crystals on all sides	DP ₃₃ heatsink fins surround entire canister
FR ₁₁ Focus on a section of the capsule	X	X	X	X

Table 2.3.1 - physically coupled design of system locality

A notable input internal design constraint was one that outlined the size of the housing where the spent nuclear waste canisters would sit. From Table 2.1.1, FR₁₁ outlined the satisfaction requirements for this constraint. The design consisted of four DPs which impacted the fulfilment of FR₁₁. Figure 2.1.2 highlights the different subsystems; cooling, sensing, electricity generation and transmission of data, which were scattered across the design. This was not a huge issue as the design would be installed on the nuclear canister before insertion into the repository, it would just result in an installation process that would take much longer than necessary and infrastructure in the repositories that would need to be modified more than necessary.

Table 2.3.2 - coupled design of protection sub-system

	DP ₄₁ Metal Casing
FR ₄₁ Protect energy harvesting devices	X
FR ₄₂ Protect sensors	X
FR ₄₃ Protect communications	X

CN₃ outlines a need for a “longevity of operation”. FR₄ subsequently requires the design “protect system from radiation”. The design outlined in Figure 2.1.2 satisfied this requirement with a metal casing that surrounded the electronic circuitry. The potential problem with that was that in the event of a potential failure of this DP, functional requirements; FR₄₁, FR₄₂ and FR₄₃ would be invalidated. The requirement for the design solution to be reliable and long lasting is an extremely important one.

Comparing the solution in Figure 2.1.2 with a completely uncoupled, theoretical solution (individual DPs for each FR), it was three times more likely to fail this requirement over a particular period of time. If the design was to work in a nuclear waste repository for the 50 - 100 years it is active, the probability of system failure had to be minimised.

The remaining yellow cells in Table 2.2.1 highlighted other areas that the design was uncoupled. Namely, the measurement of the canister condition and the transmission of data to the surface. In the case of the measurement of the canister condition, this was uncoupled due to the onboard computer's (DP_{21}) requirement for the sensor unit's (DP_{12}) information prior to measurement. Due to the ordering of these processes, this uncoupled design was unavoidable.

For the transmission of data, in the design, there was a radio transmitter (DP_{22}) which would transmit data straight to the surface. This caused the coupling of the FR_{22} and FR_{23} requirements - transmitting data out of the borehole and to the surface, respectively.

2.4 Proposed refactoring of design

From the analysis of the initial independence matrix it was evident that areas of the design needed to be improved and overhauled. Large refactors included re-thinking the locality of the design and uncoupling the protection of individual components in the system. A smaller problem was one regarding the transmission of information. As discussed in the previous section - the process of transmitting information out of the borehole and to the surface was coupled by the design transmitting information straight from the capsule to the surface. As indicated by the independence matrix, it was an area that could be decoupled.

2.5 Refactored design

The refactored design aimed to solve the problems highlighted previously by the axiomatic theory, specifically the independence axiom. Instead of sensing, electricity generation and cooling all being done on separate areas of the canister, the revamped design present in Figure 2.5.1 proposed a new solution - encapsulate all functionality and place the design on top of the canister. Here, heat dissipation was done using vertical heat rods, electricity was generated through TEG units on the face, and sensing was done above the insulating unit.

The coupling that existed with the protection measures of the previous design, no longer existed. Now, specific materials had been chosen to prevent corrosion and heat transmission.

Furthermore, the issue with the coupled design of data transmission was now only decoupled, each with a dedicated system for transmitting data out of the bore hole and up to surface.

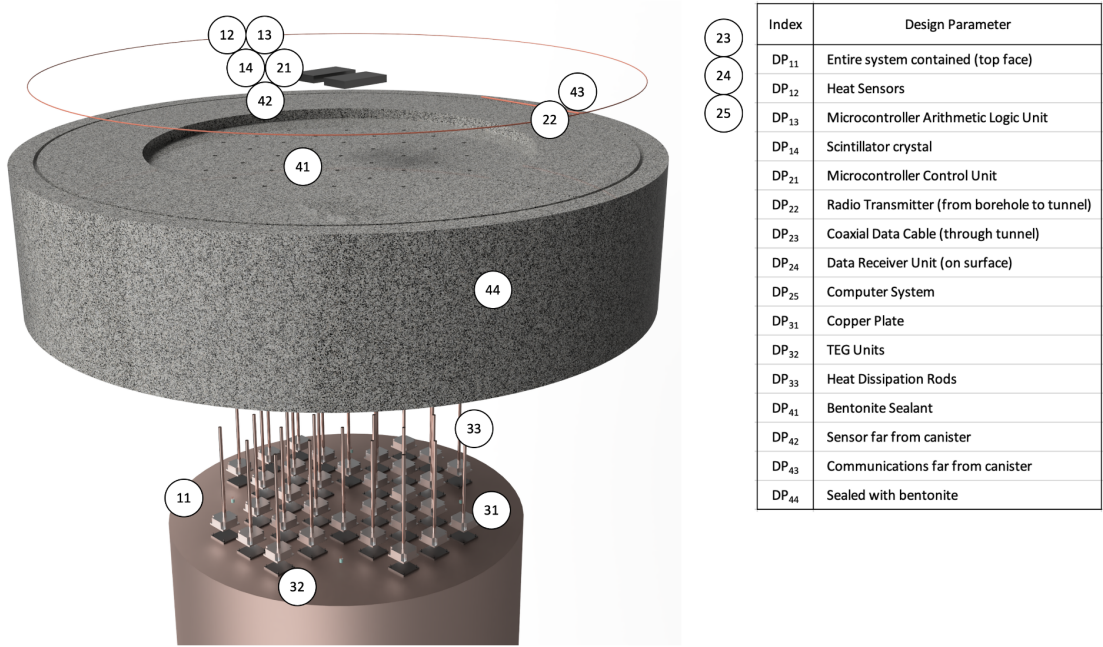


Figure 2.5.1 - refactored design with new design parameters

2.6 Reapplying the Independence Axiom

Table 2.6.1 - independence matrix for final design

	DP ₁₁	DP ₁₂	DP ₁₃	DP ₁₄	DP ₂₁	DP ₂₂	DP ₂₃	DP ₂₄	DP ₂₅	DP ₃₁	DP ₃₂	DP ₃₃	DP ₄₁	DP ₄₂	DP ₄₃	DP ₄₄
FR ₁₁	X															
FR ₁₂		X														
FR ₁₃			X													
FR ₁₄				X												
FR ₂₁					X											
FR ₂₂						X										
FR ₂₃							X									
FR ₂₄								X								
FR ₂₅									X							
FR ₃₁										X						
FR ₃₂											X					
FR ₃₃												X				
FR ₄₁													X			
FR ₄₂														X		
FR ₄₃															X	
FR ₄₄																X

When compared with the previous independence matrix, the output represented by Table 2.6.1 was far superior. For starters, there were equal functional requirements and design parameters (FRs = DPs). This was a sign that the design was uncoupled or decoupled. It was evident that FR₄ was no longer coupled, this was indicated with the strict one-to-one relationship between FRs and DPs over the FR₄ section. FR₁₁ was also no longer coupled, this was evident from the fact that DP₁₁ was the only design parameter that impacted that requirement. The only place where there was

any degree of coupling was the transmission of data, this was highlighted by the only yellow element in the matrix. The reasoning for this decoupled state was discussed in Section 2.3 - transmission of data to the surface requires the transmission of data from the canister's borehole to the main tunnel.

2.7 Reflection on using the Independence Axiom

After working out the customer needs and design constraints, the initial functional requirements were formulated. As the design progressed, the independence axiom from Axiomatic Design Theory was applied to the relationship between the design's evolving parameters and the base functional requirements. This allowed the systematic execution of the design process as it properly highlighted what aspects of the design needed to be refactored and when. As the design delved deeper into the "detailed design" section of the design process, refactoring became much more tedious and time consuming. The application of the independence axiom went great lengths to save time when designing as it ironed out design flaws earlier, when there was less at stake. Overall, the independence axiom was utilised effectively to ensure an efficient journey through the design process.

2.8 Impact of Independence Axiom on Design concepts

The Independence Axiom helped with the refinement of three design concepts. For each one, it allowed the critical evaluation of the degree to which each concept was coupled.

2.8.1 Location of design

Here, the independence axiom caused the complete overhaul of the previous system and the generation of the design that works in the final design. It highlighted the need to encapsulate all systems into one product - a design that reduces installation costs, reduces the alteration of existing infrastructure and increases overall stability of the entire system.

2.8.2 Protection of system

Previously, the solution to the protection problem was simply a metal-shielded box that contained all perishable components. The issue with the design was that if the box failed, all components were compromised. Applying the independence axiom, allowed the conclusion that all components should be individually protected. This result greatly increases the longevity of the design solution.

2.8.3 Transmission of data

What was originally a power-consumptive, high fail-rate system, became a secure, two-part system which allows the transmission of data at much lower power costs.

3. Technical Design and Analysis

3.1 Sensors

3.1.1 The Radiation Sensor

Overview

In order to monitor for leaks in nuclear waste storage, a system must be designed that can withstand the stresses of a high temperature environment for an extended period of time with high reliability. Through research and experimentation, the radiation sensor system was designed comprising of a microcontroller, a silicon photomultiplier (SiPM) optically coupled to a scintillation crystal via an curing optical coupling gel, a DC Voltage converter board that would output the high voltage required by the SiPM, and a discriminator circuit constructed out of two op-amps (OPA2354 was deemed suitable) and various resistors. Figure 3.1.1 Demonstrates how the components would be housed conceptually, relative to each other within the heat resistant ceramic housing. The total footprint of the system is 3x3x7 centimetres, and the calculated cost of components is under \$400; see Appendix A1.

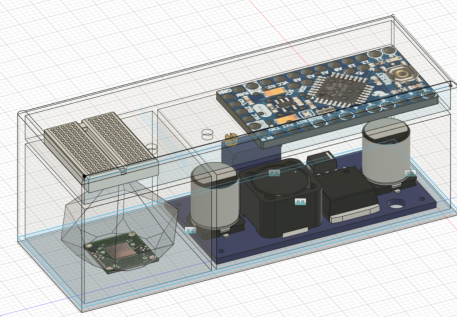


Figure 3.1.1 Render of all electronic components

3.1.1.1 Scintillation Detection

As a result of radioactive decay occurring in nuclear waste, radiation is emitted in the form of alpha and beta particles, gamma rays and neutrons.[6] Research and experimentation shows that alpha and beta particles are incapable of penetrating the nuclear waste canisters and the surrounding bentonite or earth, making them unsuitable for use in nuclear waste leak detection.

Neutrons do not carry any charge, and hence rarely interact with the waste material within the canister, meaning they are highly penetrative, more so than gamma radiation. Though released in small amounts, neutrons can penetrate through the drums of the nuclear canister and can be detected within several metres of the surrounding earth.[7]

The emitted gamma rays are also highly penetrative, and are capable of travelling through the nuclear waste canisters and the local surrounding environment, making them suitable for use in leak detection.[8]

Figure 3.1.2 illustrates the penetrative capability of these forms of emitted radiation.

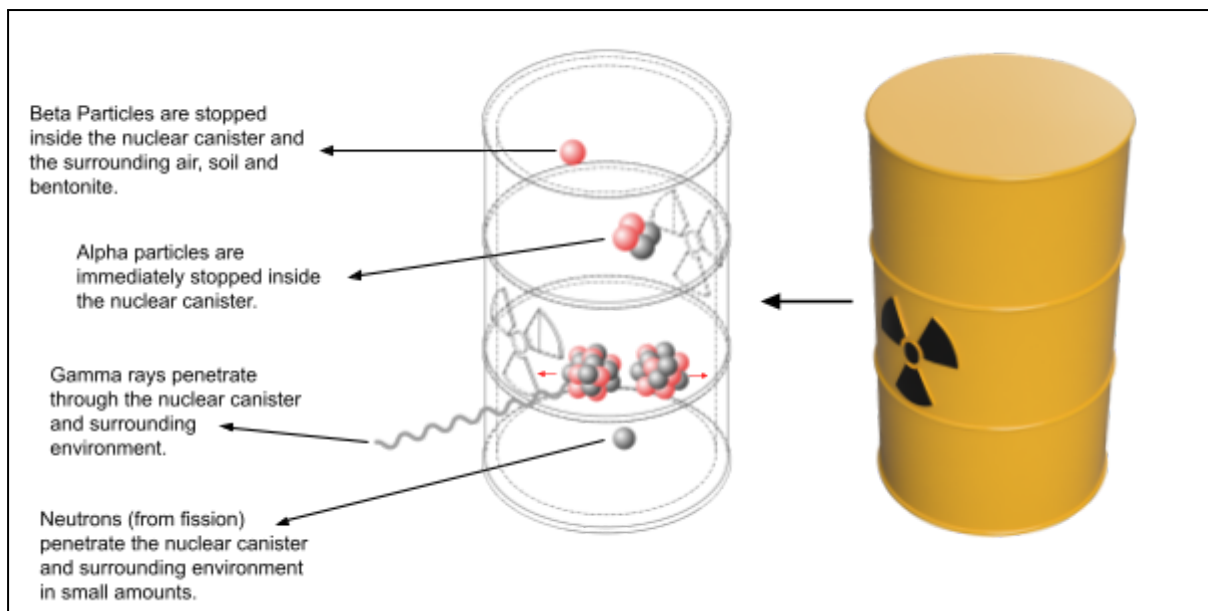


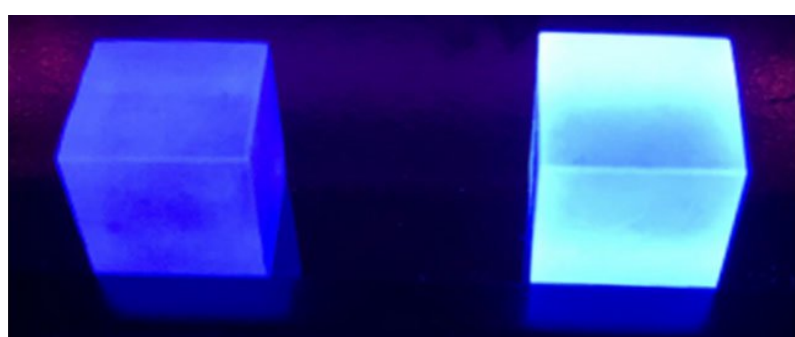
Figure 3.1.2 Sketch of the radiation forms and their penetrative ability relative to the nuclear canister.

The conclusions drawn from research indicate that the leak detection sensor system should specialise in the detection of neutrons and gamma rays.

The solution utilises scintillation crystals, a new technology employed for radiation detection in applications including X-ray security, nuclear cameras and computerised tomography (CT) scanners. The composition of scintillator crystals results in luminescence being produced when excited by coinciding ionising radiation.

Scintillator crystals come with the advantage of fast operation speed, immunity to temperature fluctuations, a low cost and consistent quality of radiation sensitivity depending on the composition of the crystal used. This is in contrast to the few alternative radiation detection methods, notably the gas-filled Geiger–Müller tube which degrade over time when exposed to heat, rendering them unsuitable for use.

Figure 3.1.3 demonstrates the effects produced by the Scintillation process when exposing a NaI crystal to UV radiation.



NaI scintillation crystal (left), NaI:Tl scintillation crystal (right) excited by a 254 nm wavelength (UV) LED lamp

Figure 3.1.3 Scintillation Crystal Excitation [17]

3.1.1.2 SiPM and Discriminator Biassing Circuit Design

The basis of the scintillator detection system involves a silicon photomultiplier (SiPM), which is responsible for the detection of nuclear radiation as indicated by the emission of light through the scintillator crystals. The SiPM converts the detected radiation into a pulse of electrical current.

The SiPM has three terminals for connection to the sensor circuit. The SiPM is biassed at the anode and cathode, and this overvoltage determines the amplitude of electrical signals from the signal output terminal. However, SiPM's have an upper limit on the bias voltage since the detection efficiency tends to saturate and the noise increases exponentially. A voltage bias of ~30V is usually best for optimum performance.

Essential to the integration of the SiPM in the system is the discriminator circuit, which converts the low level analog outputs of the SiPM into variable width Transistor-transistor logic (TTL) digital signals that can be interpreted by the microcontroller. The design of the discriminator circuit relies on a generic OP-Amp window comparator circuit design. This type of circuit interprets an analogue signal and determines whether it is within a given window of provided reference voltages, producing a lengthened 5V output that can be interpreted by the microcontroller if so. Figure 3.1.4 and 3.1.5 show the digital design of the circuit, and its logic flow diagram respectively[9]. The SiPM discriminator circuit can be seen to utilise two rail-to-rail OPA2354 op-amps.

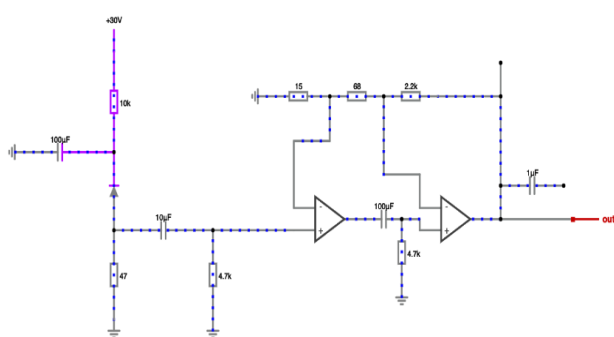


Figure 3.1.4

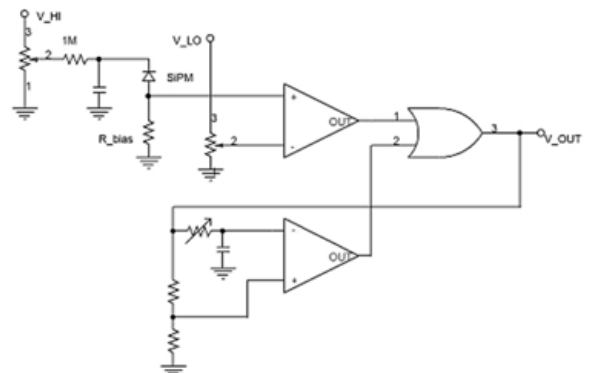


Figure 3.1.5 [9]

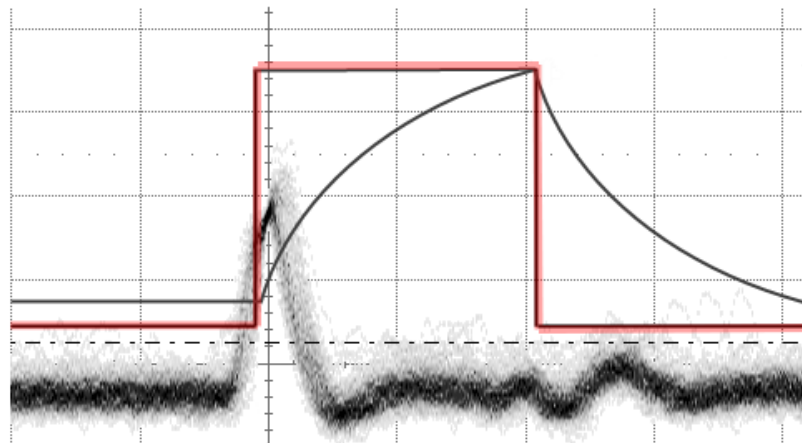


Figure 3.1.6 Output of discriminator circuit

Figure 3.1.6 demonstrates the effective output of the discriminator circuit, highlighted in red, when a small signal spike is detected from the SiPM. This line overlays the detected analogue output of the SiPM which forms the blurred line along the bottom. This lengthened and amplified digital TTL signal can be readily interpreted by the microcontroller.

3.1.1.3 Microcontroller

An Arduino Pro Mini microcontroller is programmed in C++ to accumulate the detected pulses of ionising radiation detected by the scintillation circuit in counts per minute (CPM). A threshold, or a baseline safe radiation as a result of environmental radiation without exposure to a nuclear waste leak, is first established and outputted to the data transmission module. Once established, the sensor system will detect the environmental radiation and compare the CPM to the threshold value. Depending on the requirements of the client, the system may be used strictly as an emergency alert system, or a constant monitoring system. If used for constant monitoring, the CPM values are constantly output to the transmission system for analysis by the client. If the client requires a system purely for emergency alerts; the CPM is compared to the threshold value, if it is exceeded, the radiation CPM is outputted to the data transmission module signalling the detection of a nuclear waste leak.

Figure 3.1.7 is a flowchart reflecting the operation of the scintillation sensor system for use in either case, breaking down the key components of the sensor module.

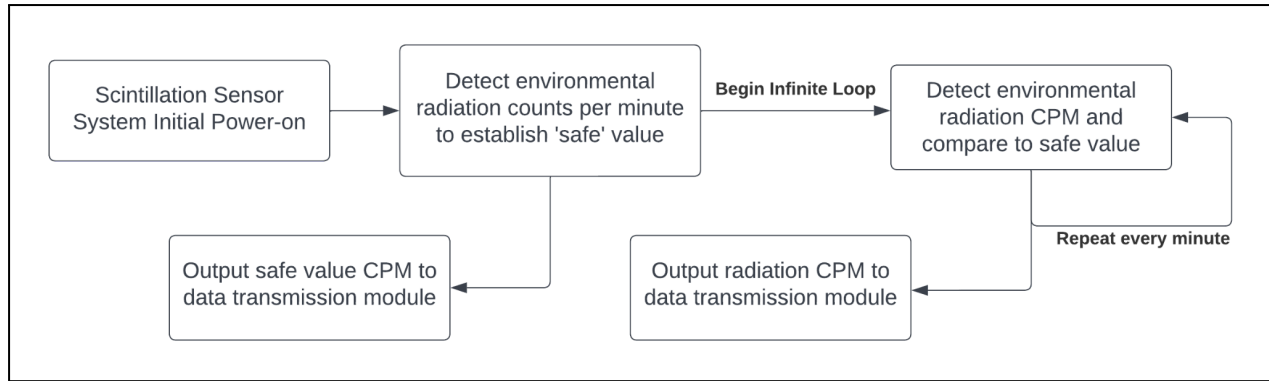


Figure 3.1.7 Scintillator sensor detection system flowchart

Experimentation was conducted by a team of engineers at the National Laboratories of Southern Catania, Italy, investigating the detection of radiation leaks in the transportation process of nuclear waste using scintillation detection. Figure 3.1.8 indicates the results from their experiment, whereby a sample detector was placed near radioactive sources. It was explained that spikes were induced in samples F, G, L, M, N and O due to short displacements of the sources near the detector.[10] From the figure however, the count rate is observed to increase at the presence of the radiation samples. Taking sample C (Cobalt-60, a radioactive isotope) for example, the count rate can be observed to increase up to approximately 16 counts per second as compared to sample A (no radioactive source) at 0 counts per second. The effectiveness of the scintillation sensor system is thus proven.

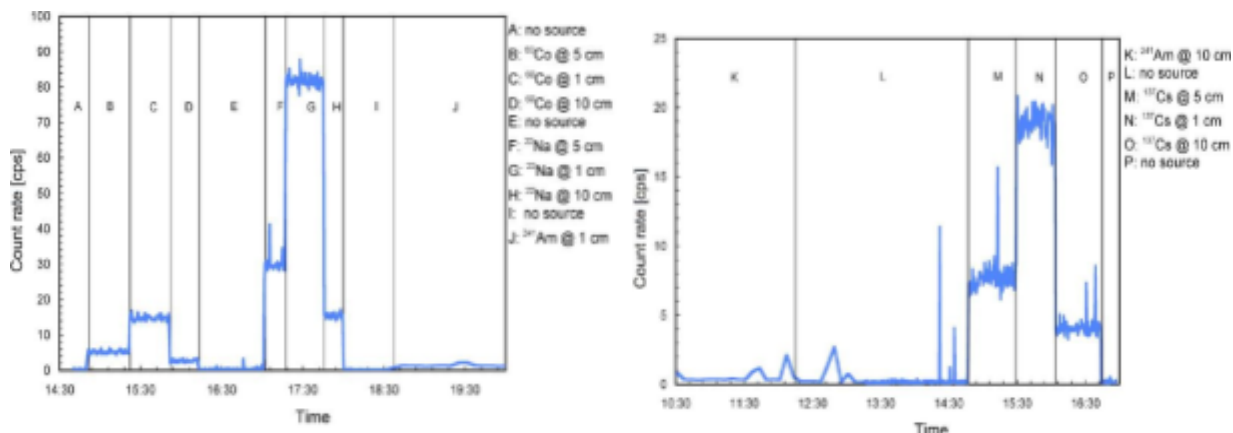


Figure 3.1.8 Graph indicating the count rate response of scintillation system at presence of different radioactive samples (A-P)

3.1.2 Scintillator Crystal Selection

LYSO is a Cerium doped Lutetium-based inorganic crystal that offers several benefits compared to many common scintillation materials. LYSO offers high density and short decay time and an exceptionally high photon-emission rate for gamma radiation detection. The peak emission wavelength is 420 nm, which is well matched

to the sensitivity curve of silicon photomultipliers. LYSO is also non-hygroscopic, which means it can be embedded in the water absorbing bentonite blocks.

3.1.3 Algorithm design for Scintillation System

Pseudocode was completed for the scintillation system, as exhibited in Figure . In summary, the code is designed to count the number of Scintillation crystal pulses per minute. The system is first initialised via the ‘setup()’ function, with the number of scintillation pulses, variable ‘counts’, set to 0. The ‘impulse()’ function runs when an interrupt occurs, whereby a scintillation pulse is detected. The function increases the number of counts by 1 each time it is called. A while loop is then entered and executed repeatedly until a minute lapses. Once completed, the number of counts is taken to be the threshold value, the baseline as a result of environmental radiation. The while loop is then terminated and exited. The function ‘loop()’ is then executed, containing an infinite loop that detects the number of counts per minute and compares the value to the threshold defined in the ‘setup()’ function. If an anomaly is detected in the process of comparison (i.e. the number of counts is 15% higher than the threshold value), then this is outputted to the data transmission module. Figure 3.1.9 contains further detailed comments regarding the operation of the pseudocode.

```

1 // This Sketch counts the number of Scintillation crystal pulses a minute.
2
3 // Connect the GND on Arduino to the GND on the Dc converter.
4 // Connect the 5V on Arduino to the 5V on the Dc converter.
5 // Connect the VIN on the Photomultiplier to the D2 on Arduino.
6
7 // Arduino doesn't support exception handling.
8
9 unsigned long counts; // variable for counting Scintillation pulses - limit of 4,294,967,295 on arduino.
10 unsigned long previousMillis; //variable for measuring time
11
12 unsigned long initialaverage; // count initial reference average value (depends no the environment).
13 // Also depends on the Scintillation crystal used.
14 // Testing with Americium-241 from a smoke detectors ion chamber made the average count was 519 CPM.
15 // This will be different in a nuclear waste geological deposit environment.
16
17 void impulse() { // called every time there is a FALLING signal on pin 2 i.e a Scintillation pulse is detected
18     counts++;
19 }
20
21 #define LOG_PERIOD 60000 // count rate currently 1 minute / longer times may case counts exceed 4,294,967,295
22 // causing overflow errors.
23
24 void setup() { // Initial setup
25     counts = 0;
26     Serial.begin(9600); // prints counts to the console, this code will later be output to DATA TRANSMISSION MODULE
27
28     pinMode(2, INPUT); // Read input from pin 2. Break in the high input is one Scintillation pulse detected.
29
30     attachInterrupt(digitalPinToInterrupt(2), impulse, FALLING); //define external interrupts.
31     // Interruption on the signal to pin 2 runs the impulse function.
32     Serial.println("Start initial average counter"); // starts counting initial average minute value
33
34     unsigned long currentMillis = millis();
35     bool minute = false;
36     while (minute == false) { // Creates an infinite loop that halts everything except interrupts from happening.
37         if (currentMillis - previousMillis > LOG_PERIOD) {
38             previousMillis = currentMillis;
39             initialaverage = counts; // count the 'safe' CPM value. Depents on location relative to radiation sources
40             counts = 0;
41             minute = true;
42         }
43     }
44 }
45
46 void loop() { // Infinite Cycle, detects Scintillation pulses every minute
47     unsigned long currentMillis = millis();
48     if (currentMillis - previousMillis > LOG_PERIOD) { // Every 60 seconds
49         previousMillis = currentMillis; // Reset Millisecond counter
50         Serial.println(counts); // prints counts to console, this will later become output to DATA TRANSMISSION MODULE.
51         counts = 0;
52     }
53 }

```

Figure 3.1.9 C++ code for the scintillation sensor system

3.1.4 Power Analysis for the Radiation Sensor

The overall power usage of the system depends on its current state and environment, hence a best and worst case of power usage are to be calculated, this ensures quantitatively that the power consumption of the sensor system does not exceed the capabilities of the TEG power generation system.

The electronic components and their determined power consumption in the Sensor system include the following:

The Arduino Pro Mini comes in two models that can be powered with either a regulated 3.3V or 5V supply (depending on the model) on the Vcc pin. There is a voltage regulator on board so it can accept voltage up to 12VDC. Since the minimum input to the XL6009 DC converter board is 5V, it is logical to use the 5V arduino platform throughout, which draws 26mA at idle and thus consumes 0.013W at idle.[11] Under load the microcontroller is limited to a current draw of 500mA total, which may be encroached upon with temperature increase, hence the maximum power that can be used by the microcontroller is 2.5W.[12]

Data is limited on the general power consumption of Silicon Photomultipliers, as it is very little and often considered negligible in systems. Power dissipated at idle is 0.4W according to research on their application in the medical industry[13]. This power consumption would increase very slightly as signals are detected and output, though this is insignificant in comparison to the power consumption of the DC converter which amplifies the low level output signal with some inefficiency.

The last power consuming element in the system is the DC step up power module which provides the high voltage required for the SiPM to detect signals via the photoelectric effect. This component remains at idle until a photon signal is detected, meaning the power consumption results from inefficiencies in the DC voltage step-up conversion process. The idle current draw is 18mA for the XL6009 board used in the system and the minimum provided voltage from the Arduino is 5V, meaning the passive power consumption is 0.09W.

When under load, the energy efficiency of the board is rated at 94% and the maximum input current draw is 4A, this may be met by the SiPM depending on the model and the detection rate of incident radiation. Under this worst case scenario of constant detection load, the maximum power usage of the system can be calculated to be;

$$4A * 30V (\text{output voltage}) * 0.94 (\text{conversion efficiency}) = 7.2W$$

The overall power consumption of the system due to its components is summarised in table 3.1.10, the total power consumption of the system is 10.1 Watts under maximum load, meaning it is comfortably within the capabilities of the TEG power generation solution.

Table 3.1.10 Power Consumption Summary

	Sensor System Component			
	Arduino Pro Mini	SiPM Silicon Photomultiplier	XL6009 DC Voltage Converter	Total (Watts)
Idle Power Consumption (Watts)	0.013	0.4	0.09	0.503

Worst Case Power Consumption (Watts)	2.5	0.4	7.2	10.1
--------------------------------------	-----	-----	-----	------

3.2 Material Selection

3.2.1 Thermal Requirements of Materials

Thermoelectric generators (TEGs) produce power through a temperature delta across its body. To maximise power generation, the temperature delta must as well be maximised. The thermal evolution of the canister and the surrounding rock is known and thus the purpose of the cooling apparatus surrounding the TEGs is to place the 'hot' side of the TEG on the greatest temperature available, and the 'cool' side on the lowest.

With thousands of different TEGs on the market, the one chosen for this design needed to be optimised for a lower temperature differential which is uncommon as most are made for the highest possible power generation from the most amount of temperature difference. As shown on graph 3.2.1, the temperature difference for canister to rock even after 100 years is shown to be at 45 degrees celsius with higher temperatures in the previous years.

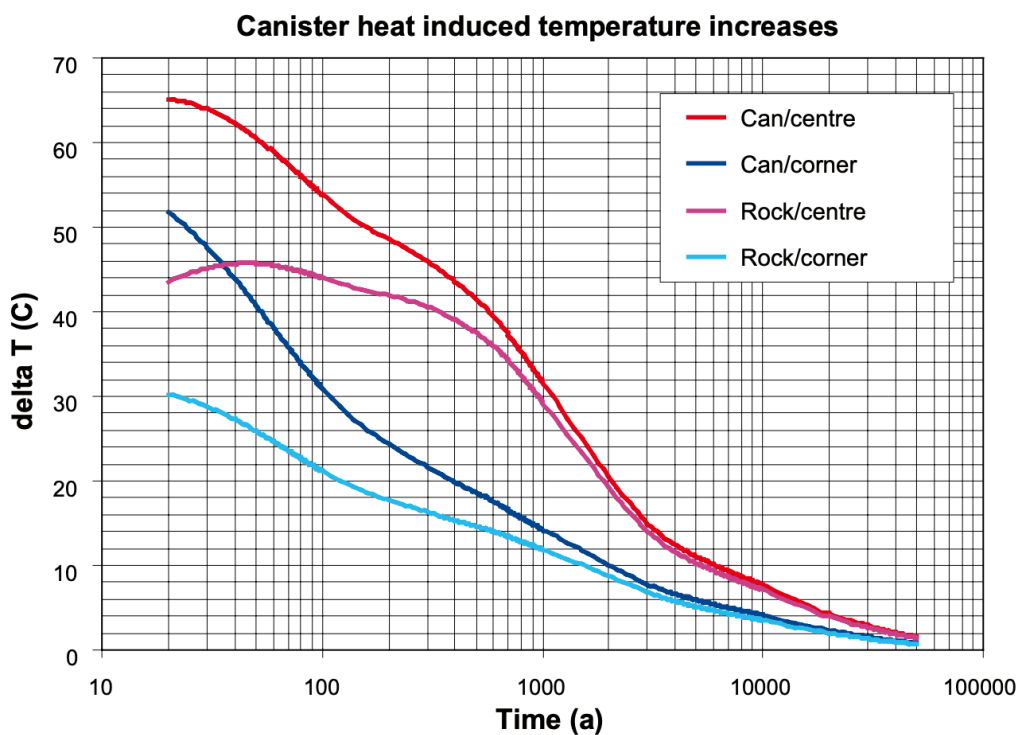


Figure 3.2.1 Temperature difference of 45°C after 100 years

Based on this, a TEG that can produce power from a temperature differential of around 34 degrees celsius will be optimal for this design. This temperature is found in section 3.2.1.2 from the heat loss from the thermal connection and thermal insulation. The selection of the TEG for this design is a 6-watt TEG module, 4V

output, 30 mm square which for each is 21\$ and as shown in the graph 3.2.2, can produce around 1 watt per TEG at the temperature difference of around 45 degrees celsius. From this, the design will have 32 of these TEGs to allow around 32 watts of power needed to power the sensor system.

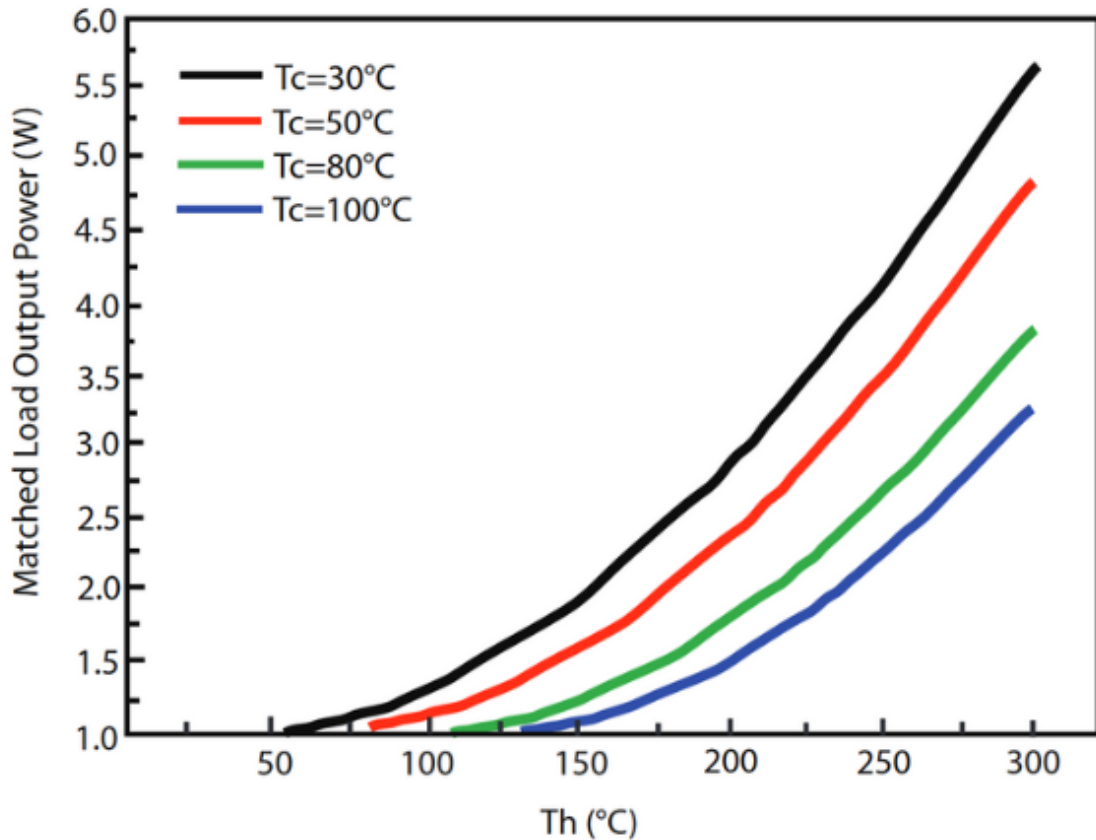


Figure 3.2.2 Relationship between temperature delta and power

The greatest temperature found in the environment is the surface of the waste canister so the trivial solution is to place the ‘hot’ side of the TEG directly on the canister. The temperature of the surrounding rock gradually decreases as the distance to the canister increases. To minimise the temperature on the ‘cool’ side,

1. A section of cool rock the furthest viable distance from the canister must be efficiently thermally connected to the TEG and,
2. Isolated from its hot surroundings.

3.2.1.1 Thermally Connecting Rock to TEGs

The highest thermal conductivity as well as the lowest specific heat capacity will be essential for the power generation in the design, the material selected for connecting the TEGs to the rocks must follow these two parameters whilst also maintaining a reasonable price for the design.

The following are the best material options for the heat rod:

Table 3.2.3 Material characteristics for thermal transfer

Material	Thermal Conductivity (W/m*k)[14]	Specific Heat capacity (J/g K)[15]	price
Aluminium	247	0.900	1.50\$/kg
Copper	398	0.386	5\$/kg
Diamond	2200	0.54	50 million usd/kg
Gold	315	0.126	80 thousand usd/kg
Heat pipe	5,000-100,000	0.350	20\$ per pipe

Clearly from the options within table 3.2.3, heat pipes are the optimal choice for the thermal transfer between the TEGs and the rock due to the insanely high thermal conductivity and the reasonably low specific heat capacity and price.

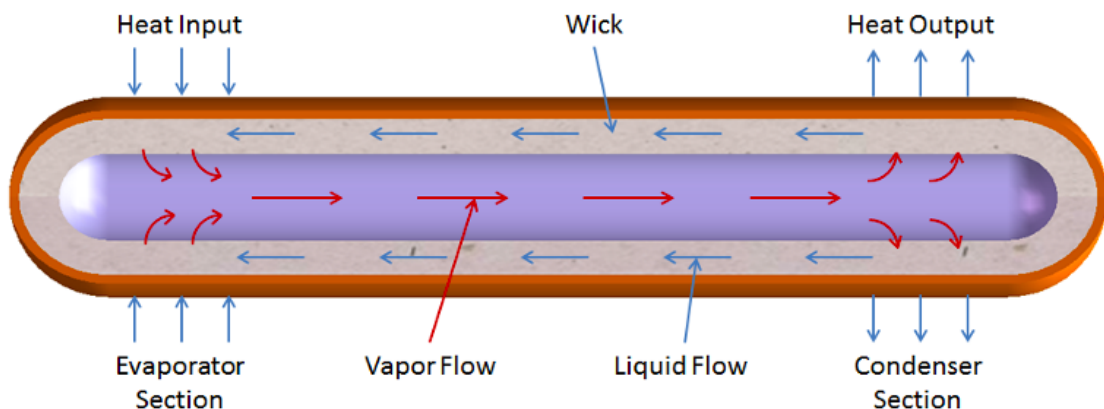


Figure 3.2.4 cross section of a heat pipe

To confirm this, thermal simulations were completed comparing the three most viable heat transfer materials, Heat Pipe, Solid Copper and Solid Aluminium.

The simulations were run on a single unit cell of the device (seen in *Figure 3.2.5*) using a copper plate at the bottom at $T = 85^\circ\text{C}$ to emulate the canister surface, and the surrounding rock temperature was applied to the heat rod's (variable material) surface at $T = 40^\circ\text{C}$. These temperature values were taken from the estimated temperature at $t = 100$ years. The material and material properties of other components were estimated and constant throughout the 3 simulations and thus this

study is purely comparative, testing the viability of the heat conducting material not actual temperature differentials achieved by the device. The final temperature differential will be found after all thermal materials are chosen.

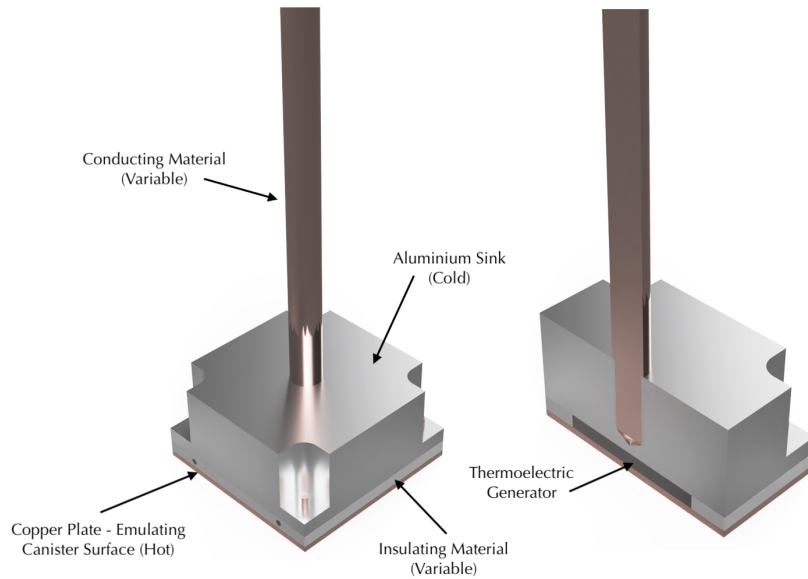


Figure 3.2.5 Left: Unit cell of power generation device. Right: Cross section of unit cell showing encased thermoelectric generator.

Thermal simulations results;

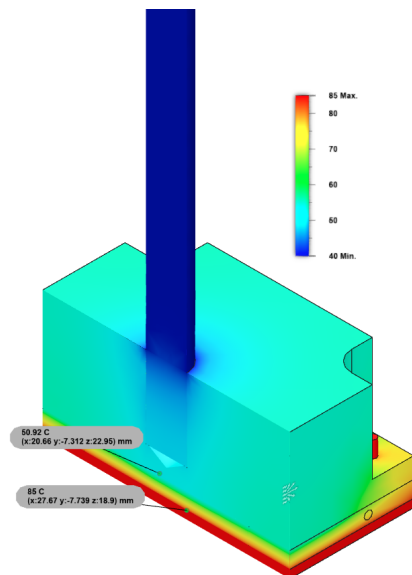


Figure 3.2.6 Thermal simulation using heat pipe.

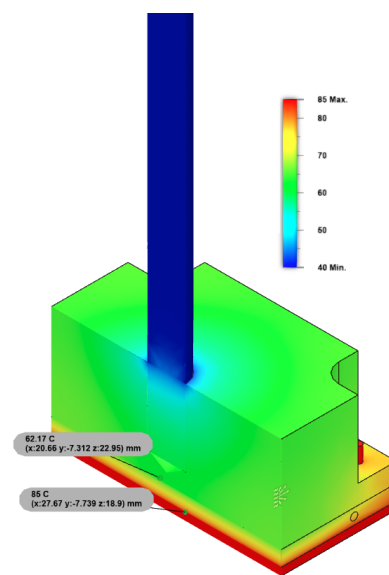


Figure 3.2.7 Thermal simulation using solid copper pipe.

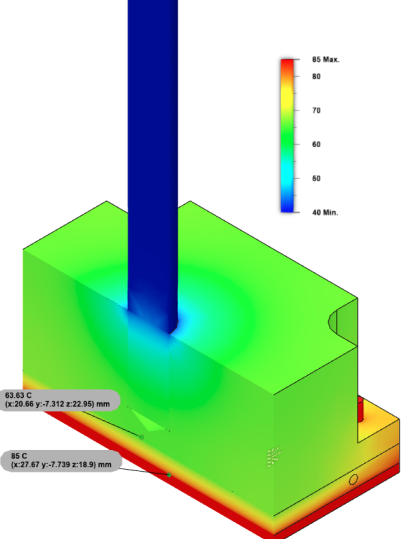


Figure 3.2.8 Thermal simulation using solid aluminium pipe.

Table 3.2.9 Results from Thermal Simulations

Property	Heat Pipe	Solid Copper	Solid Aluminium
Thermal Conductivity	5000 W/mK (Minimum)	398 W/mK	247 W/mK
Specific Heat	0.350 J/gK	0.386 J/gK	0.900 J/gK
T_{Hot}	85°C	85°C	85°C
T_{Cold}	50.92°C	62.17°C	63.63°C
ΔT	34.08°C	22.83°C	21.37°C

As seen in table 3.2.9, the temperature differential achieved by the heat pipe is 50% and 60% greater than solid copper and solid aluminium respectively and thus heat pipes will be used as the thermal conductor into the rock.

3.2.1.2 Thermal Isolation

The insulation required for the heat pipe requires a material that is both low in thermal conductivity as well as having a high specific heat capacity, this will be essential for the production of energy within the design.

The following are the best possible options for the thermal insulation:

Table 3.2.10 Material characteristics of thermal insulators

Material	Thermal Conductivity (W/m*k)	Specific Heat capacity (J/g K)	Price
Clay	0.37	0.84	\$7/kg
Water	0.598	4.186	Free
Plastic	0.33	0.54	\$2/kg
Cellular glass	0.08	0.84	\$20/m^2
Bentonite	0.58	1.25	\$6.64/kg

From the options within table 3.2.10, water and plastic cannot be used for this design, this is because water can potentially spread leaked waste into the

surrounding environment and plastic will not last the 100,000 years that these chambers need to be maintained for. Thus the best option would be Cellular glass due to the extremely low thermal conductivity as well as the most reasonable specific heat capacity and price. Another benefit of the cellular glass is that it is an inorganic solution meaning it will be able to last for very long times within the depositories and never have any negative effects on the chambers.

To confirm this, thermal simulations were completed comparing the three most viable heat insulating materials, Cellular Glass, Clay and Bentonite. The simulation setup is identical to the previous simulations except the heat pipe is held constant while the insulating material is varied.

Thermal simulations results;

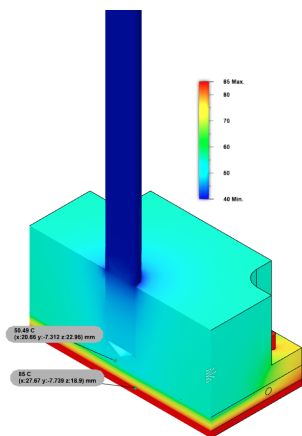


Figure 3.2.11 Thermal simulation using Cellular glass.

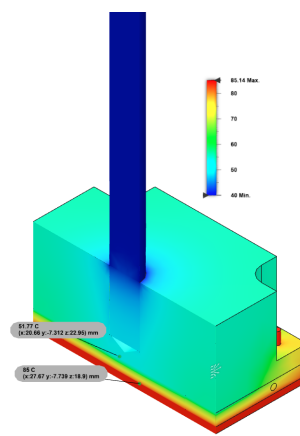


Figure 3.2.12 Thermal simulation using bentonite.

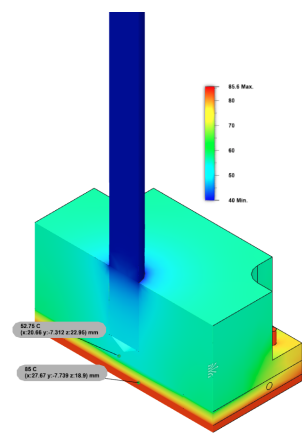


Figure 3.2.13 Thermal simulation using insulating clay.

Table 3.2.14 Results from Thermal Simulations

Property	Cellular Glass	Bentonite	Insulating Clay
Thermal Conductivity	0.08 W/mK	0.58 W/mK	0.37 W/mK
Specific Heat	0.840 J/gK	1.25 J/gK	0.840 J/gK
T_{Hot}	85°C	85°C	85°C
T_{Cold}	50.49°C	51.77°C	52.75°C
ΔT	34.51°C	33.23°C	32.25°C

From the results in table 3.2.14, the temperature differential is optimised using Cellular glass as the insulating material however the temperature difference between the insulating materials is minimal and the major difference comes from the material selected for the heat conductor.

After thermal material optimisation, using heat pipes for the thermal transfer of heat away from the TEG to the rock, and using Cellular Glass to insulate the TEG from the canister, the final temperature differential per unit cell of the device is;

$$\Delta T = 34.51^\circ C.$$

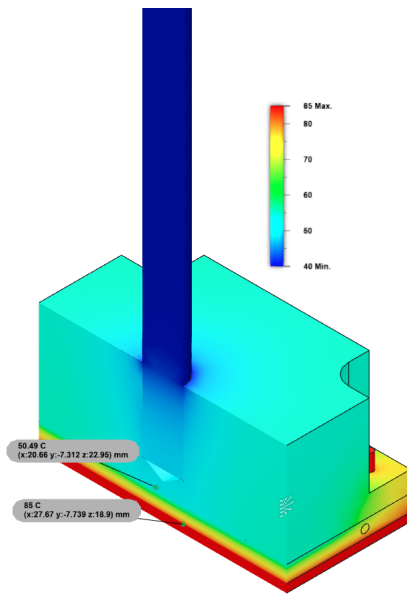


Figure 3.2.15 Thermal simulation giving final temperature delta.

Bentonite is also an important material to discuss for the design as the chambers within these tunnels are already planned to be filled with it. This will be optimal due to its low thermal conductivity and reasonable specific heat capacity resulting in the perfect environment as a thermal insulator for the heat production from the TEGs. Bentonite is also the perfect seal for these depositories due to how it can absorb large amounts of water which is essential as any form of liquid in these environments have the potential of spreading the harmful radioactive waste into the surrounding environment.

3.2.2 Strength Requirements of Materials

For the strength requirements for the design, the optimal material would be a low cost and high strength option. This is due to the distributed load directly on top of the device, with the bentonite clay filling in the containment area and placing said force axially on the simplified cylindrical structure of the housing.

From the graph 3.2.16, by using the a minimum threshold for strength (red line) within the relative cost to strength graph, the optimal selection for the material can be chosen. [16]

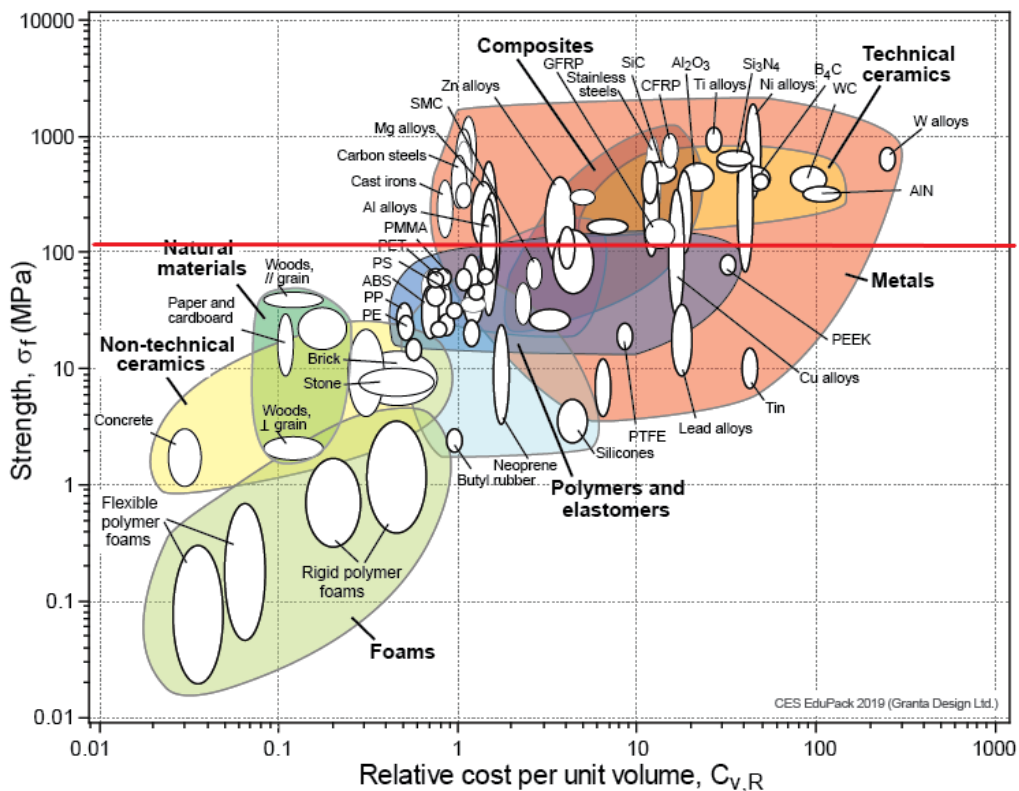


Figure 3.2.16 strength - relative cost/volume chart

From previous thermal analysis, copper and aluminium alloys would be the optimal material for the design whilst within the strength against relative cost per unit graph 3.2.16, copper and aluminium alloys have quite a high strength with it being above the red line which is the minimum strength requirement for this design as well as being a reasonable cost per unit. Therefore the material selected for the majority of the aspects within the design are aluminium due to the higher strength with the heat pipes being made from copper due to the higher thermal conductivity as well as high strength. Both these materials also have a high resistance to corrosion which will be optimal for these deep depositories where no maintenance can be done.

3.2.3 Non-Epoxy Material for Circuitry

As the sensor system and circuitry will be exposed to high temperatures for an extended period of time, it will experience rapid degradation. PCB materials used currently throughout industry, namely FR-4 glass-reinforced epoxy laminate, has an expected lifespan of 50 - 70 years when used within the manufacturer's specified conditions.

This makes the material less than ideal for use in the required application, with a factor of unpredictability as to the lifespan of the circuitry which is integral to the operation of the leak detection.

From the various electronic components in the system, a PCB can be formed that accommodates and appropriately connects all the required voltage regulators, SOCs, resistors and diodes of each individual component.

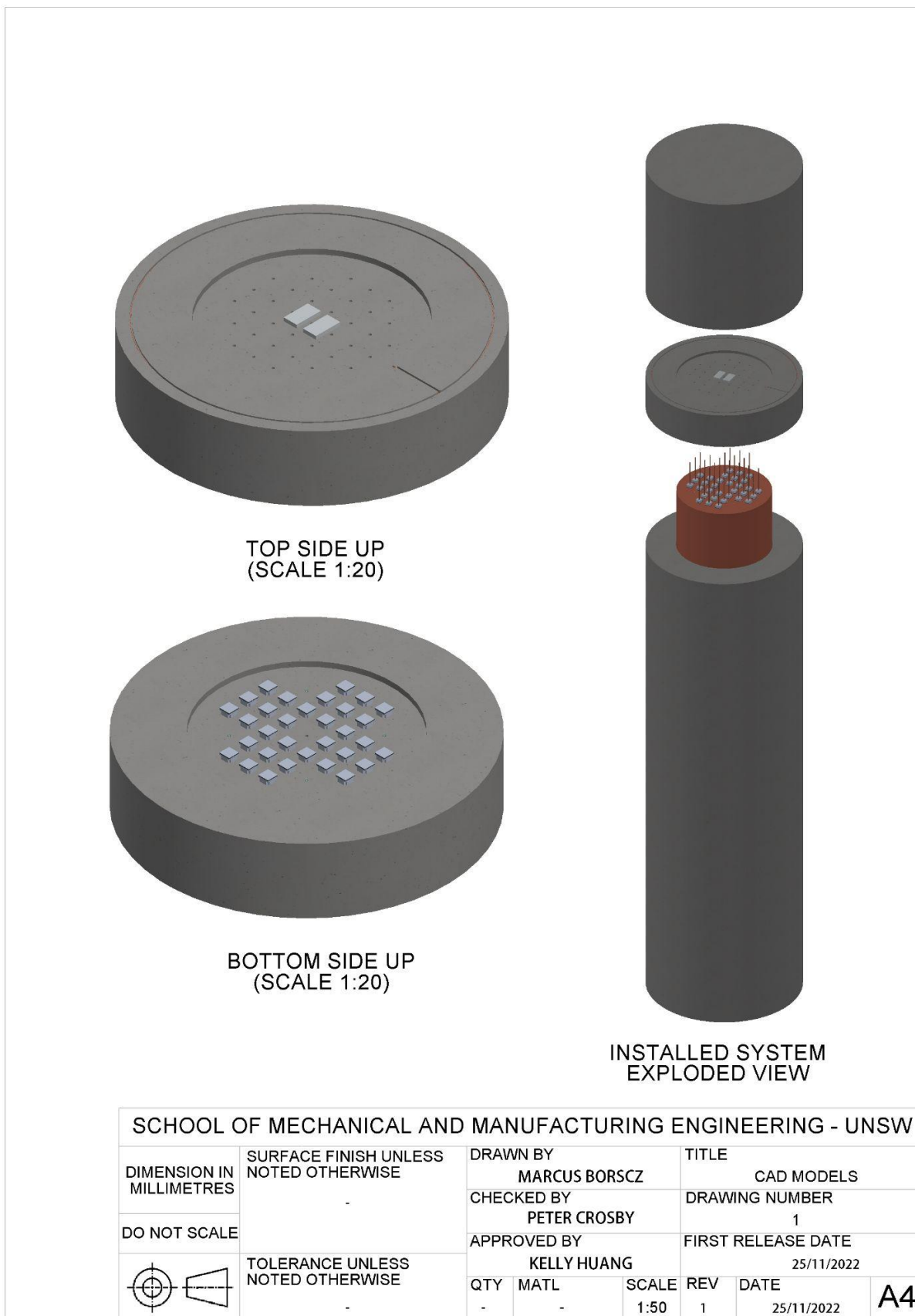
The ideal material for this PCB would be Ceramic with Silicon Nitride as its substrate; this material can easily have a circuit printed on it, and is notable for its high thermal resistance and hardness, making it suitable for use in applications requiring high reliability such as military weapons control systems, aviation and spacecraft.

Silicon Nitride (Si_3N_4) material properties:

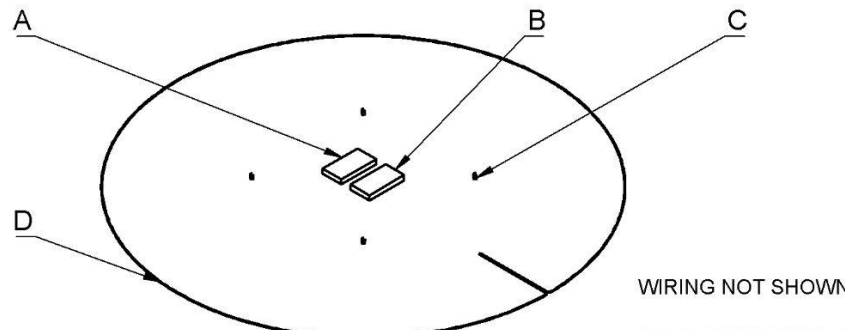
Table 3.2.17 Silicon Nitride material properties

Thermal Expansion	~ 3.3 ppm/ $^{\circ}\text{C}$
Thermal Conductivity	30 - 32 W/mK
Max. Temperature	$\leq 1150^{\circ}\text{C}$
Resistance	$\geq 10^{10} \Omega\text{cm}$
Compressive Strength	~ 2500 MPa

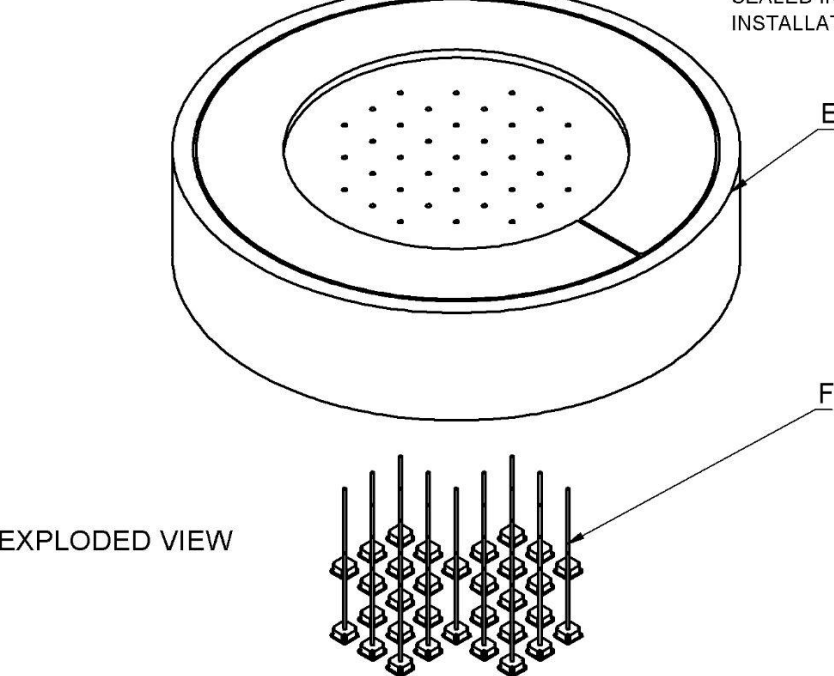
4. CAD Model and Mechanical Part Drawing



PART	NAME	QTY.	DRAW. NO.	DESCRIPTION
A	CIR-1	1	-	SENSING CIRCUIT
B	CIR-2	1	-	COMMUNICATION CIRCUIT
C	SEN-1	4	8	RADIATION SENSOR
D	RNG-1	1	-	TRANSMITTER COIL
E	BLK-1	1	3	MONITORING BLOCK
F	HAR-1	32	4	ENERGY HARVESTING ASSEMBLY

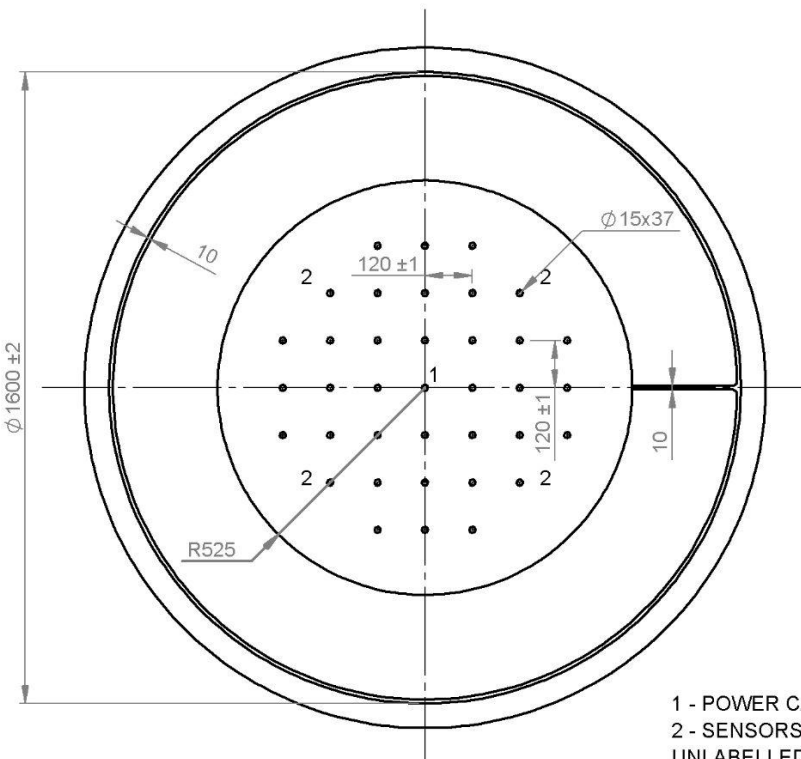


ALL COMPONENTS ARE
SEALED IN BENTONITE AFTER
INSTALLATION



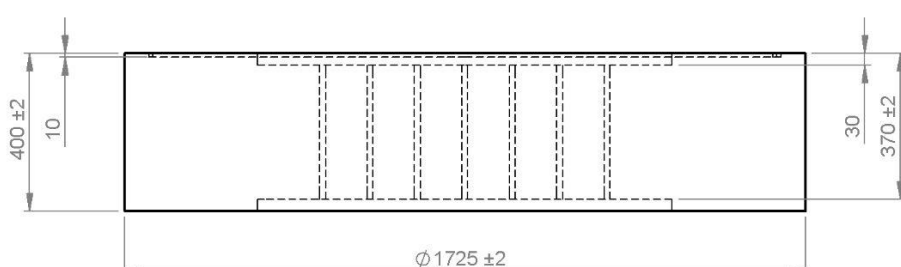
SCHOOL OF MECHANICAL AND MANUFACTURING ENGINEERING - UNSW

DIMENSION IN MILLIMETRES	SURFACE FINISH UNLESS NOTED OTHERWISE	DRAWN BY		TITLE	
		MARCUS BORSCZ		MONITORING SYSTEM	
DO NOT SCALE	TOLERANCE UNLESS NOTED OTHERWISE	CHECKED BY		DRAWING NUMBER	
		PETER CROSBY		2	
APPROVED BY		FIRST RELEASE DATE			
KELLY HUANG		25/11/2022			
	-	QTY	MATL	SCALE	REV
		1	-	1:18	1
A4					



TOP VIEW

1 - POWER CABLES
2 - SENSORS
UNLABELLED - HEAT PIPES

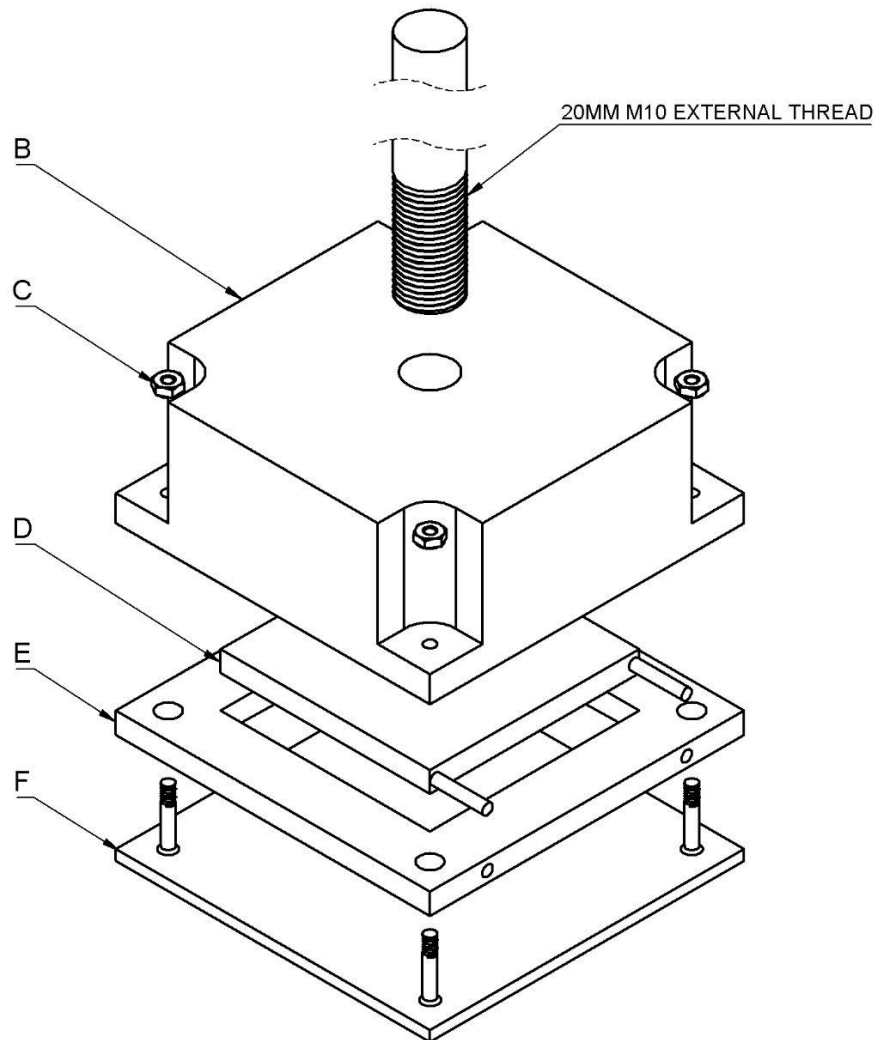


SIDE VIEW

SCHOOL OF MECHANICAL AND MANUFACTURING ENGINEERING - UNSW

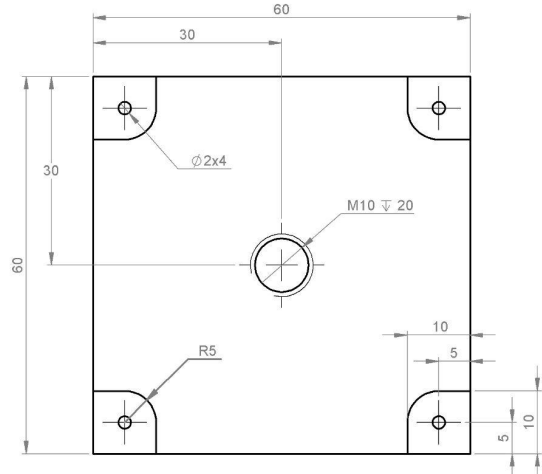
DIMENSION IN MILLIMETRES	SURFACE FINISH UNLESS NOTED OTHERWISE 	DRAWN BY MARCUS BORSCZ		TITLE MONITORING BLOCK BLK-1	
		CHECKED BY JORDAN WHITTAKER		DRAWING NUMBER 3	
DO NOT SCALE	APPROVED BY 	KELLY HUANG		FIRST RELEASE DATE 25/11/2022	
	TOLERANCE UNLESS NOTED OTHERWISE ±0.5 MM	QTY 1	MATL BETNONITE	SCALE 1:15	REV 1 DATE 25/11/2022 A4

PART	NAME	QTY.	DRAW. NO.	DESCRIPTION
A	WTV-124675	1	-	HEAT PIPE $\varnothing 10 \times 300\text{MM}$
B	HAR-1A	1	5	COLD SIDE
C	M2-HFA2-S100-	4	-	M2 NUT
D	SP1848	1	-	TEG 40x40x4MM
E	HAR-1B	1	6	INSULATION
F	HAR-1C	1	7	HOT SIDE

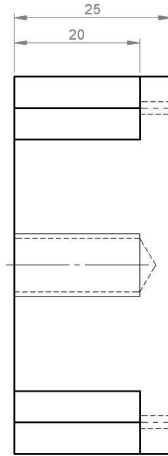


SCHOOL OF MECHANICAL AND MANUFACTURING ENGINEERING - UNSW

DIMENSION IN MILLIMETRES	SURFACE FINISH UNLESS NOTED OTHERWISE	DRAWN BY		TITLE	
		MARCUS BORSCZ		ENERGY HARVESTER HAR-1	
DO NOT SCALE	TOLERANCE UNLESS NOTED OTHERWISE	CHECKED BY		DRAWING NUMBER	
		JORDAN WHITTAKER		4	
		APPROVED BY		FIRST RELEASE DATE	
		KELLY HUANG		25/11/2022	
		QTY	MATL	SCALE	REV
		32	-	5:4	1
					DATE
					25/11/2022
					A4

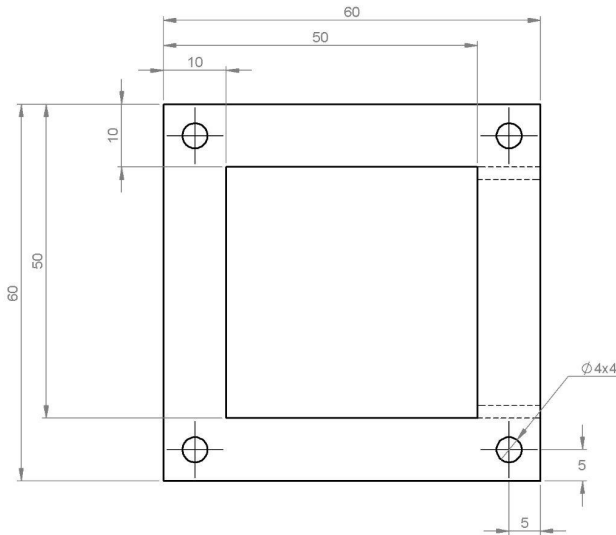


TOP VIEW

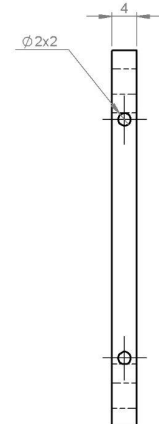


SIDE VIEW

SCHOOL OF MECHANICAL AND MANUFACTURING ENGINEERING - UNSW			
DIMENSION IN MILLIMETRES	SURFACE FINISH UNLESS NOTED OTHERWISE	DRAWN BY	TITLE
DO NOT SCALE	✓	MARCUS BORSZC CHECKED BY JORDAN WHITTAKER APPROVED BY KELLY HUANG	COLD SIDE HAR-1A DRAWING NUMBER 5 FIRST RELEASE DATE 25/11/2022
	TOLERANCE UNLESS NOTED OTHERWISE 0.5 MM	QTY 32 MATL ALUM. 5052	SCALE 3:2 REV 1 DATE 25/11/2022 A4

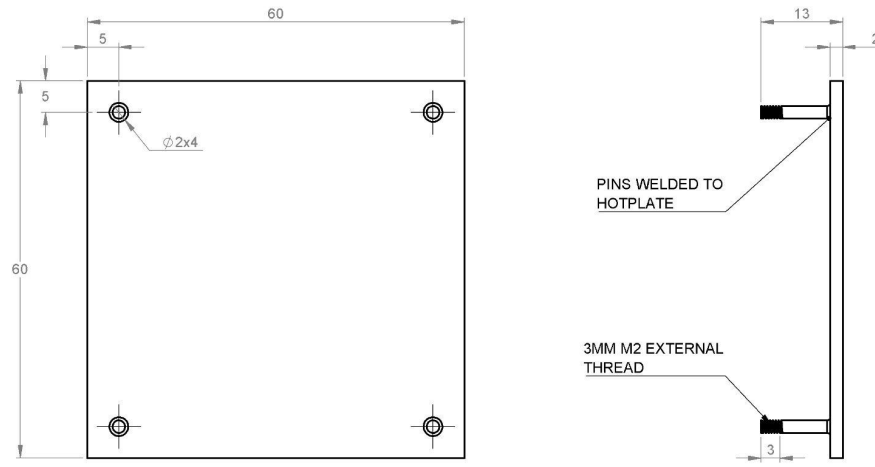


TOP VIEW



SIDE VIEW

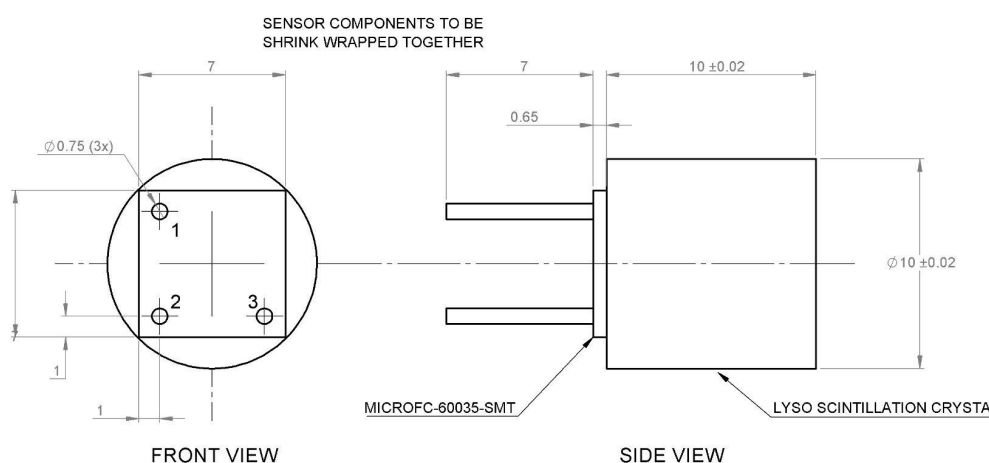
SCHOOL OF MECHANICAL AND MANUFACTURING ENGINEERING - UNSW			
DIMENSION IN MILLIMETRES	SURFACE FINISH UNLESS NOTED OTHERWISE	DRAWN BY	TITLE
DO NOT SCALE	✓	MARCUS BORSZC CHECKED BY JORDAN WHITTAKER APPROVED BY KELLY HUANG	INSULATION HAR1-B DRAWING NUMBER 6 FIRST RELEASE DATE 25/11/2022
	TOLERANCE UNLESS NOTED OTHERWISE ±0.5 MM	QTY 32 MATL FOAM GLASS	SCALE 3:2 REV 1 DATE 25/11/2022 A4



TOP VIEW

SIDE VIEW

SCHOOL OF MECHANICAL AND MANUFACTURING ENGINEERING - UNSW			
DIMENSION IN MILLIMETRES	SURFACE FINISH UNLESS NOTED OTHERWISE	DRAWN BY	TITLE
DO NOT SCALE	✓	MARCUS BORSZC CHECKED BY JORDAN WHITTAKER APPROVED BY KELLY HUANG	HOT SIDE HAR-1C DRAWING NUMBER 7 FIRST RELEASE DATE 25/11/2022
	TOLERANCE UNLESS NOTED OTHERWISE ±0.1 MM	QTY 32 MATL ALUM. 5052	SCALE 3:2 REV 1 DATE 25/11/2022 A4



FRONT VIEW

SIDE VIEW

PIN #	DESCRIPTION
1	CATHODE
2	FAST OUTPUT
3	ANODE

SCHOOL OF MECHANICAL AND MANUFACTURING ENGINEERING - UNSW			
DIMENSION IN MILLIMETRES	SURFACE FINISH UNLESS NOTED OTHERWISE	DRAWN BY	TITLE
DO NOT SCALE	-	MARCUS BORSZC CHECKED BY DANIEL ARENA APPROVED BY KELLY HUANG	RADIATION SENSOR SEN-1 DRAWING NUMBER 8 FIRST RELEASE DATE 25/11/2022
	TOLERANCE UNLESS NOTED OTHERWISE ±0.05 MM	QTY 4 MATL -	SCALE 5:1 REV 1 DATE 25/11/2022 A4

5. Conclusion

The automated leak detection system outlined holds great potential to succeed as an engineering solution to the defined gap in the market, which is an absence of a monitoring capability in deep geological nuclear waste repositories. The uniqueness of the solution stems from its self-sustained operation via thermal energy harvesting, a method not fully explored in the market of nuclear radiation detection. From an experiment that demonstrated the effectiveness of scintillation systems for nuclear radiation detection, to a thermal simulation that validated the power output generation, evidence-based models in this report proved the feasibility of the final design concept.

Though faced with many design constraints, whether it involved regulations imposed by the IAEA or material constraints due to the nature of the repositories and the nuclear waste canisters, these challenges were overcome through multiple models and iterations of the design. The application of the independence axiom theory and methods such as morph matrices assisted significantly to the final solution, ruling out undesirable design effects whilst satisfying the customer needs and functional requirements. The system was also well under the \$10000 budget and is definitely cost effective given the critical nature of such a project.

Though the timeline of the project was rather condensed, specifications for the design have been reasonably finalised. Future work may see the development of a working small-scale prototype to test the final design solution, with refinements taken as may be required. If successful, the automated leak detection system could see a greater investment in permanent deep geological repositories as a result of increased community confidence and safety.

References

- [1] "What is nuclear energy?" [Online]. Available: <https://whatisnuclear.com/>. [Accessed 5 Nov. 2022].
- [2] IEA, "Nuclear - Fuels & Technologies" 17 Oct. 2022 [Online]. Available: <https://www.iea.org/fuels-and-technologies/nuclear>. [Accessed 5 Nov. 2022].
- [3] Investor Group on Climate Change, "International Energy Agency Net Zero Emissions Scenario" [Online]. Available: https://igcc.org.au/wp-content/uploads/2021/07/IGCC-IEANZE_BriefingPaper_FINAL.pdf. [Accessed 5 Nov. 2022].
- [4] IRENA, "Global Energy Transformation: A Roadmap to 2050" [Online]. Available: https://www.irena.org/-/media/Files/IRENA/Agency/Publication/2018/Apr/IRENA_Report_GET_2018.pdf. [Accessed 10 Nov. 2022].
- [5] Science, "Finland built this tomb to store nuclear waste. Can it survive 100000 years?" 24 Feb. 2022, [Online]. Available: <https://www.science.org/content/article/finland-built-tomb-store-nuclear-waste-can-it-survive-100000-years>. Accessed 5 Nov. 2022.
- [6] Research Outreach, "Providing better radiation monitoring for nuclear waste," *Research Outreach*, 03-Aug-2022. [Online]. Available: <https://researchoutreach.org/articles/providing-better-radiation-monitoring-nuclear-waste>. [Accessed: 15-Nov-2022].
- [7] "Neutron radiation," *Wikipedia*, 30-Oct-2022. [Online]. Available: https://en.wikipedia.org/wiki/Neutron_radiation. [Accessed: 15-Nov-2022].
- [8] P. Finocchiaro., "DMNR: A New Concept For Real-Time Online Monitoring Of Short And Medium Term Radioactive Waste", *Radioactive Waste: Sources, Types and Management*, 2011.
- [9] "Particle detection with Silicon Photomultipliers," *Electronics - Particle Detection with Silicon Photomultipliers*. [Online]. Available: http://mfp.physics.umn.edu/s07/Projects/S07_CosmicShowerDecoherence/electronics.html. [Accessed: 15-Nov-2022].
- [10] P. Finocchiaro, "Radioactive waste: A system for online monitoring and data availability," *Nuclear Physics News*, vol. 24, no. 3, pp. 34–39, 2014.
- [11] J. S. Cook, "Arduino Pro Mini Low Power Tutorial," *Arrow.com*, 13-Oct-2022. [Online]. Available: <https://www.arrow.com/en/research-and-events/articles/getting-started-with-the-arduino-pro-mini>. [Accessed: 18-Nov-2022].
- [12] "Reducing arduino power consumption," *Reducing Arduino Power Consumption - SparkFun Learn*. [Online]. Available: <https://learn.sparkfun.com/tutorials/reducing-arduino-power-consumption/all>. [Accessed: 18-Nov-2022].
- [13] G. Maira, M. Mazzillo, S. Libertino, G. Fallica, and S. Lombardo, "Crucial aspects for the use of silicon photomultiplier devices in continuous wave functional near-infrared spectroscopy," *Biomedical Optics Express*, vol. 9, no. 10, p. 4679, 2018.

- [14] "Top 10 thermally conductive materials," *Thermtest*, 02-Jun-2021. [Online]. Available:
<https://thermtest.com/thermal-resources/top-10-resources/top-10-thermally-conductive-materials>. [Accessed: 18-Nov-2022].
- [15] Libretexts, "T4: Specific heats and molar heat capacities," *Chemistry LibreTexts*, 14-Jul-2020. [Online]. Available:
https://chem.libretexts.org/Ancillary_Materials/Reference/Reference_Tables/Thermo_dynamics_Tables/T4%3A_Specific_Heats_and_Molar_Heat_Capacities. [Accessed: 85-Nov-2022].
- [16] M. F. Ashby, *Materials selection in mechanical design*. Amsterdam: Butterworth-Heinemann, 2017.
- [17] Research (no date) WG2: *Crystal Growing - Center for Underground Physics*. Available at: <https://cupweb.ibs.re.kr/en/research/working-groups/crystal-growing/> [Accessed: 18-Nov-2022].

Biography

Ben Kernohan Second year student B Computer Science/ B Mechatronics Engineering (Honours)	Kelly Huang Second year student B Mechatronics Engineering (Honours)
Daniel Arena Second year student B Computer Science/ B Mechatronics Engineering (Honours)	Marcus Borscz Third year student B Mechanical Engineering (Honours)/ B Advanced Physics (Honours)
Harry Rudd Second year student B Aerospace Engineering (Honours)	Peter Crosby Second year student B Mechanical Engineering (Honours)
Jordan Whittaker Second year student B Aerospace Engineering (Honours)/ B Advanced Physics (Honours)	

Appendix

A1. Bill of Materials

Name	Qty.	Description	Material	Mass (kg)	Source	Cost
WTV-124675	32	Heat Pipe Ø10x300mm	Copper	9.82	Wakefield Thermal	\$693.12
M2-HFA2-S100-	128	M2 Hex Nut	Stainless Steel	0.02	TR Fastenings	\$11.52
SP1848	32	TEG 40x40x4 mm	Alumina	0.8	Thermal Enterprises	\$278.43
MICROFC-60035	4	Silicon Photomultiplier	Silicon	-	Onsemi	\$558.24
LYSO Crystal	4	Scintillator Ø10x10mm	LYSO Ce	0.09	EPIC Crystal	\$440.00
HAR-1A	32	EH Cold Side	Alum. 5052	7.78	Crazy Deals Online	\$398
HAR-1B	32	EH Insulation	Foam Glass	0.27	FoamGlas	\$2.00
HAR-1C	32	EH Hot Side	Alum. 5052	0.62	AliExpress	\$61.92
Electrical Cables	10 m	Mica braided wire	Mica	1	AliExpress	\$47.58
CIR-1	1	Sensing Circuit	-	0.5	In House	\$250
CIR-2	1	Comms Circuit	-	0.5	In House	\$250
				21.4		\$2,990.81